AD-A023 295

WAVES, RAYS AND DISCRIMINANTS

Freeman Gilbert

California University

Prepared for:

Air Force Office of Scientific Research

31 October 1975

REPORT DOCUMENTATION PAGE		READ INSTRUCTIONS BEFORE COMPLETING FORM
1. REPORT NUMBER AFOSR - TR - 76 - 0398	2. GOVT ACCESSION NO.	3. RECIPIENT'S CATALOG NUMBER
4. TITLE (and Subtitle) Waves, Rays and Discriminants		5. TYPE OF REPORT & PERIOD COVERED Final Technical 10/01/73 - 9/30/75
		6. PERFORMING ORG. REPORT NUMBER
7. AUTHOR(s) Freeman Gilbert		8. CONTRACT OR GRANT NUMBER(s) AFOSR-74-2621
9. PERFORMING ORGANIZATION NAME AND ADDRESS The Regents of the University of California San Diego, California 92093		10. PROGRAM ELEMENT, PROJECT, TASK AREA & WORK UNIT NUMBERS AO 1827-21 Code 5F10 Element 62701E
11. CONTROLLING OFFICE NAME AND ADDRESS Advanced Research Projects Agency Nuclear Monitoring Research Office Arlington, Virginia 22209		12. REPORT DATE 31 October 1975
		13. NUMBER OF PAGES 76
14. MONITORING AGENCY NAME & ADDRESS(if different from Controlling Office) Air Force Office of Scientific Research 1400 Wilson Boulevard Arlington, Virginia 22209		15. SECURITY CLASS. (of this report) Unclassified
		15a. DECLASSIFICATION DOWNGRADING SCHEDULE

16. DISTRIBUTION STATEMENT (of this Report)

Approved for public release, distribution unlimited

17. DISTRIBUTION STATEMENT (of the abstract entered in Block 20, if different from Report)

18. SUPPLEMENTARY NOTES

TECH, OTHER

19. KEY WORDS (Continue on reverse side if necessary and identify by block number)

Seismology, Discriminant, Moment tensor, Source mechanism, Network, Digital seismograph, Matched filtering, Deconvolution

20. ABSTRACT (Continue on reverse side if necessary and identify by block number)

A method has been developed for retrieving the seismic source mechanism by using a sparse network of seismographic stations. The method is based on matched filtering followed by deconvolution for the seismic moment tensor. The method requires well-calibrated instruments. The seismic moment tensor is decomposed into its deviatoric (earthquake-like) and isotropic (explosion-like) parts which together form a basis for discrimination. Very preliminary applications of the method are successful and encouraging, but the full potential of the method has not been established.

DD FORM 1 JAN 73 **1473** EDITION OF 1 NOV 65 IS OBSOLETE

Final Report for AFOSR Grant

This research project covered the period 1 October 1973 - 30 September 1975. The fundamental problem addressed was the discrimination between earthquakes and explosions. At the outset it became clear that data of high quality would be needed for a quantitative method of discrimination based on the seismic source mechanism. Consequently, a comparison was made among available, digitally recorded seismographs. Very preliminary results are presented in Appendix A. It appears that the SRO instruments are definitely superior to the HGLP instruments although both suffer from unexplained non-linearities. Finite loop gain may be the explanation for the SRO instrument. At long periods the fed-back LaCoste-Romberg gravimeter is the best instrument tested.

To retrieve the seismic source mechanism from observed spectra one uses the concepts of matched filtering and deconvolution. Before the beginning of this project it was known that the relationship between the seismic moment tensor and observed spectra is a *linear* one (Gilbert, 1971). It was also known, in principle, how to retrieve the moment tensor (Gilbert, 1973). The basic ideas were refined and used to retrieve the moment tensors of two, large deep earthquakes (Dziewonski and Gilbert, 1974; Gilbert and Dziewonski, 1975). The major drawback to the method was its requirement of a large, dense, global network of stations. Clearly, a method for a regional or local array was needed. Such a method was discovered as the project drew to a close and the theoretical basis for it is presented in Appendix B. In theory, one needs only a single, horizontally polarized instrument or two, vertically polarized instruments. Numerical experiments with synthetic data indicate that as few as 5-10 verticals permit retrieval down to magnitude $m = 6$.

A practical application of this novel method is presented in Appendix C where it is shown how one can use only 10 WWSSN stations to retrieve the mechanism of a deep earthquake. Digital data of sufficient quality - the instruments *must* be well calibrated - were simply not available for explosions. Therefore, a practical evaluation of this method awaits the forthcoming SRO data which is expected to be of very high quality (however, see Appendix A).

Fundamental to the application of the matched filtering method is the facility to calculate very accurate synthetic seismograms, including the effects of dissipation, for a broad range of frequencies and wave numbers. Among all known methods the classical procedure of summation of normal modes was found to be the most reliable. To compute the required normal mode eigenfrequencies and eigenfunctions is not a trivial task, even after 20 years of theoretical and numerical effort. We have found that the classical Rayleigh-Ritz procedure is the cheapest and most accurate. All eigendata with periods between 40 sec and 1 hour - about 5000 modes - can be computed for a few thousand dollars. The present programs are designed to produce the complete spectrum for all periods greater than 20 sec. The theoretical basis for this variational calculation is given in Appendix D.

At periods on the order of a few tens of seconds the concept of standing waves, valuable at longer periods, is better replaced by the concept of traveling waves. An exact theoretical traveling wave representation is presented in Appendix E. Such a representation is very desirable for applying the matched filtering methods to a regional or local network.

In summary, a novel method, based on matched filtering, has been found for retrieving the seismic source mechanism, the moment tensor, from a sparse network of instruments. The moment tensor can be examined for its deviatoric

(earthquake-like) and isotropic (explosion-like) components. Almost all earthquakes are thought to have a nearly completely deviatoric moment tensor, and almost all explosions to have an isotropic one. Thus, the unique partition of the seismic moment tensor into its deviatoric and isotropic parts provides a quantitative, unambiguous method for discriminating between earthquakes and explosions. The matched filtering method for retrieving the seismic moment tensor works. It is new and its limitations have not been explored. Clearly, it is scientifically most desirable that the full potential of this method be assessed.

Appendix A

We present some preliminary comparisons among instruments for the WWSSN, HGLP, SRO and IDA networks. The comparisons are incomplete yet adequate enough to show some of the features of the different systems.

In Figure A1 we have four seismograms of the Korean earthquake (m_b = 6.5) on September 29, 1973. The four instruments (all verticals) are: the Goodkind-Prothero superconducting gravimeter, the La Coste-Romberg gravimeter (the IDA instrument), the HGLP vertical and the WWSSN long-period vertical (recorded digitally). The HGLP vertical is located in Albuquerque, N.M. and the other three at the Piñon Flat Observatory, Calif. The two gravimeters are band-pass filtered to enhance (x100) the acceleration in the band 1 min-30 min. The HGLP vertical has the standard "noise notch" filter and the WWSSN vertical has the standard response. Rayleigh wave packets through R6 are clearly visible on the two gravimeters.

In Figure A2 we have the spectra for the first day after the earthquake from the seismograms in Figure A1 (the WWSSN spectrum is from a hand-digitized record of the Albuquerque WWSSN instrument). The filters on the two gravimeters are virtually identical in the pass band and so are the spectra of the two instruments. The similarity between the two of the spectral peaks and troughs indicates a S/N ratio approaching 50 db. At low frequencies, near 10 cph, the WWSSN vertical has a S/N ratio of at least 25 db, equal to, if not better than, the HGLP instrument. This comparison shows that a digitally recorded WWSSN vertical is at least marginally preferable to the "A" channel of the HGLP vertical and that the two gravimeters are some 25 db better than either of the

other two instruments. It is not clear whether the other two instruments respond to ground noise at long periods because the dynamic range of the recording system is taken by the large amplitude, short period motion. In the present configuration ground noise could be as much as 25 db below instrument noise at long periods for both the WWSSN and HGLP instruments.

In Figure A3 we have spectra for the second day of the earthquake. The WWSSN spectrum has been omitted. A glance at Figure A1 shows that the ambient noise level is reached some 6 hours after the earthquake for this instrument. A number of long period fundamental modes and high-Q overtones are clearly present in the spectra of the two gravimeters and, to a lesser extent, in the HGLP spectrum. At 10 cph the spectral level has dropped 15 db from day 1 to day 2 for the gravimeters and 30 db for the HGLP instrument. This demonstrates the nonlinearity of the HGLP instrument. Large amplitude, short period motions are non-linearly "aliased" to long periods. As the short period motions decay, and they decay more rapidly than the long period motions, the aliased long period motions also decay more rapidly than the true long period motions. Thus, much of the long period spectral energy in the HGLP spectra in Figures A2 and A3 is non-linearly aliased short period spectral energy. This intolerable situation makes the HGLP instrument unacceptable for long period studies.

To improve the comparison of the HGLP and La Coste instruments at long periods we turn our attention to the boom channel, channel "B", of the HGLP instrument.

In Figure A4 we have the tide channel (flat in acceleration) of the La Coste gravimeter operating in Ñaña, Peru and in Figure A5 the

"B" channel of the HGLP instrument at La Paz, Bolivia, both for the Solomon Islands earthquake, $M = 7.8$, July 20, 1975. Notice that the La Coste is recorded as an acceleration indicator and the HGLP as a displacement indicator, so that the two records have tides that are of opposite signs. In both instruments the large tidal signal takes most of the dynamic range of the recording system, leaving a few tens of "least count" for this rather large event. The desirability of band-pass filtering is obvious, and in Figure A6 we show the La Coste record amplified ×100 in the band 1 min - 30 min. This amplification is done by active filters *before* digitization so that the earthquake has a few thousands of "least count", or about 70 db, dynamic range. Spectra corresponding to Figures A5 and A6 are shown in Figures A7 and A8. Two spectra are presented in each figure, one for the 24 hr period before the earthquake and the other for the first 24 hours after the earthquake. At long periods the La Coste gravimeter has a S/N ratio for this event of about 50 db while the HGLP S/N ratio is nowhere more than 15 db. The noise level must thus be at least 35 db above ground noise; some of this is presumably least-count noise, but nonlinearity in the sensor (folding higher-frequency ground noise to lower frequencies) and noise in the instrument are also contributing.

Data for the SRO instruments has only very recently become available. Therefore, a detailed comparison of the SRO instrument with others is not now possible. We have in Figure A9 the seismogram of the Solomon Islands event recorded on the SRO vertical at Albuquerque. Although this instrument is fedback (electromagnetically) the output

is filtered with a sharp rolloff at long periods before digitization.
We have low passed the original record with a corner at 100 sec. to
obtain Figure A9. Spectra for the day before and for the first 24 hours
of the earthquake are shown in Figure A10. The S/N ratio at long
periods is 40 to 50 db, about equivalent to the La Coste gravimeter.

The lack of structure in the earthquake spectrum for periods
longer than about 300 sec is attributable to the unusually large Rayleigh
wave, R1, for the main shock. This signal represents an instrumental
problem; whether the active filters are saturated or there are difficulties
in the gain ranging, R1 as recorded on the SRO instrument appears to
be anomalous. Excising R1 from the seismogram leads to the spectra
shown in Figure A11 (the noise spectrum is the same as in Figure A10).
The spurious long-period noise disappears, and mode peaks can be seen
out to 470 seconds. Saturation is a problem with any seismographic
instrument. For the La Coste gravimeter saturation at R1 appears to be
a problem at teleseismic distances for magnitudes $M > 7\frac{1}{2}$. For the SRO
instrument the problem of saturation is not yet well understood.

At the longest periods at which modes are visible on the SRO
spectrum, the S/N ratio is only 25 db, compared with 40 db for the
La Coste. Indeed, the S/N ratio for the SRO instrument begins to deteriorate
for periods longer than 300 seconds, whereas the La Coste response remains
good out to 600 seconds. As a result, the longest-period mode unequivocally
visible on the SRO spectrum is $_0S_{13}$ at 474 seconds; on the La Coste
spectrum $_0S_5$ is visible, at a period of 1190 seconds. Another indication
of the quality of the La Coste gravimeter is presented in Figure A12.

We have four sections of the seismogram (amplified ×100 in the band
1 min - 30 min) for the Solomon Islands event spaced roughly half a
day apart. The semi-diurnal tide is evident in this figure. The
start times of the records are -8.5, +16, +28, and +41 hours with
respect to the origin time of the earthquake. Up to 2 days after this
M-7.8 event there is still evidence of the free oscillations of the
Earth.

In conclusion, it appears that the La Coste-Romberg gravimeter
is the instrument of choice for a sparse, long-period network. If
Project IDA, or a similar project also using La Coste instruments, is
not supported then seismologists will not have high-quality, long-period,
digital data. Obviously, such data are very desirable. The only other
instrument that might possibly be useful for long-period seismology is
the SRO instrument (Peterson, *et al*., USGS preprints, July-August 1975).
At present little is known about the noise characteristics
of the SRO instrument at very long periods, nor are the nonlinearities
caused by large signals well understood. It thus seems that the fedback
La Coste is the only proven low-noise vertical seismometer at very
long periods.

FIGURE CAPTIONS

Appendix A

A1.   Seismograms from the North Korean earthquake of September 29, 1973, recorded on a La Coste gravimeter and superconducting gravimeter, and standard Press-Ewing, at Piñon Flat Observatory, and an HGLP at Albuquerque.

A2.   Spectra from the first 24 hours after the North Korean earthquake.

A3.   Spectra from the second 24 hours after the North Korean earthquake.

A4.   Solomon Islands earthquakes of July 20 and 21, 1975 recorded on the tide channel of the La Coste gravimeter at Ñaña, Peru.

A5.   The Solomon Islands earthquakes on the B Channel of the HGLP at La Paz, Bolivia.

A6.   The Solomon Islands earthquakes on the Ñaña La Coste gravimeter with the band   .3 to 10 mHz amplified by 100.

A7.   Power spectrum of the Solomon Islands earthquakes on the HGLP B channel. Light line is for 24 hours before the earthquake; heavy line is for 24 hours after.

A8.   Power spectrum from the NNA x 100 record.

A9.   Solomon Islands earthquakes, recorded on the SRO vertical at Albuquerque; data have been digitally lopassed to remove frequencies above 10 mHz.

A10.   Power spectra of the seismogram in A9. (Light line is spectrum
of previous 24 hours.)

A11.   Power spectrum of signal in A9, but with R1 excluded.

A12.   Signal from x100 output of NNA La Coste at times before and
after Solomon Islands earthquakes, to show rate of signal decay.

NORTH KOREA
Sept. 29, 1973 m_b = 6.5

SC
PFO

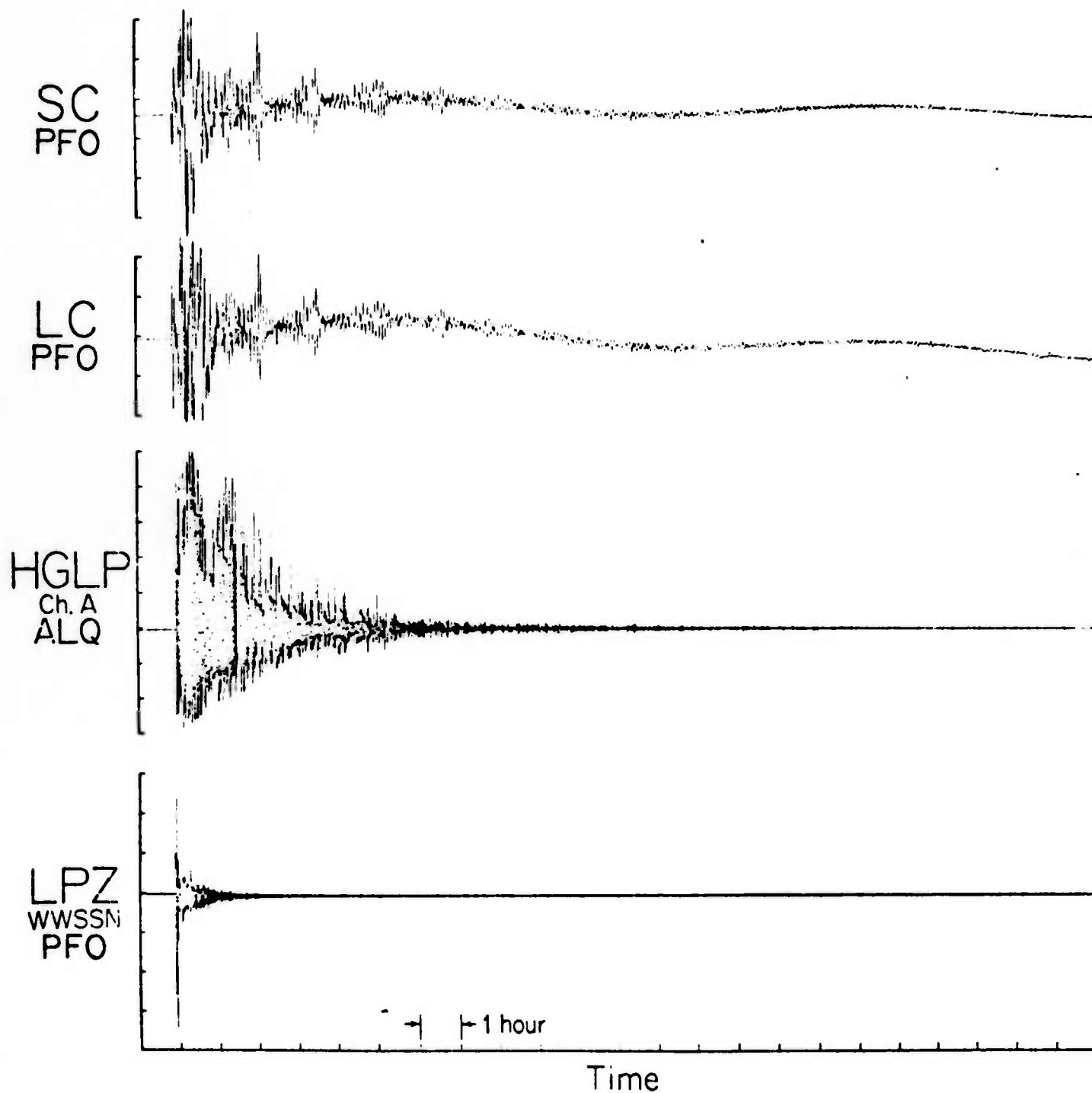LC
PFO

HGLP
Ch. A
ALQ

LPZ
WWSSN
PFO

⊢1 hour

Time

Figure A1

NORTH KOREA
Sept. 29, 1973 $m_b = 6.5$
(Day 1)
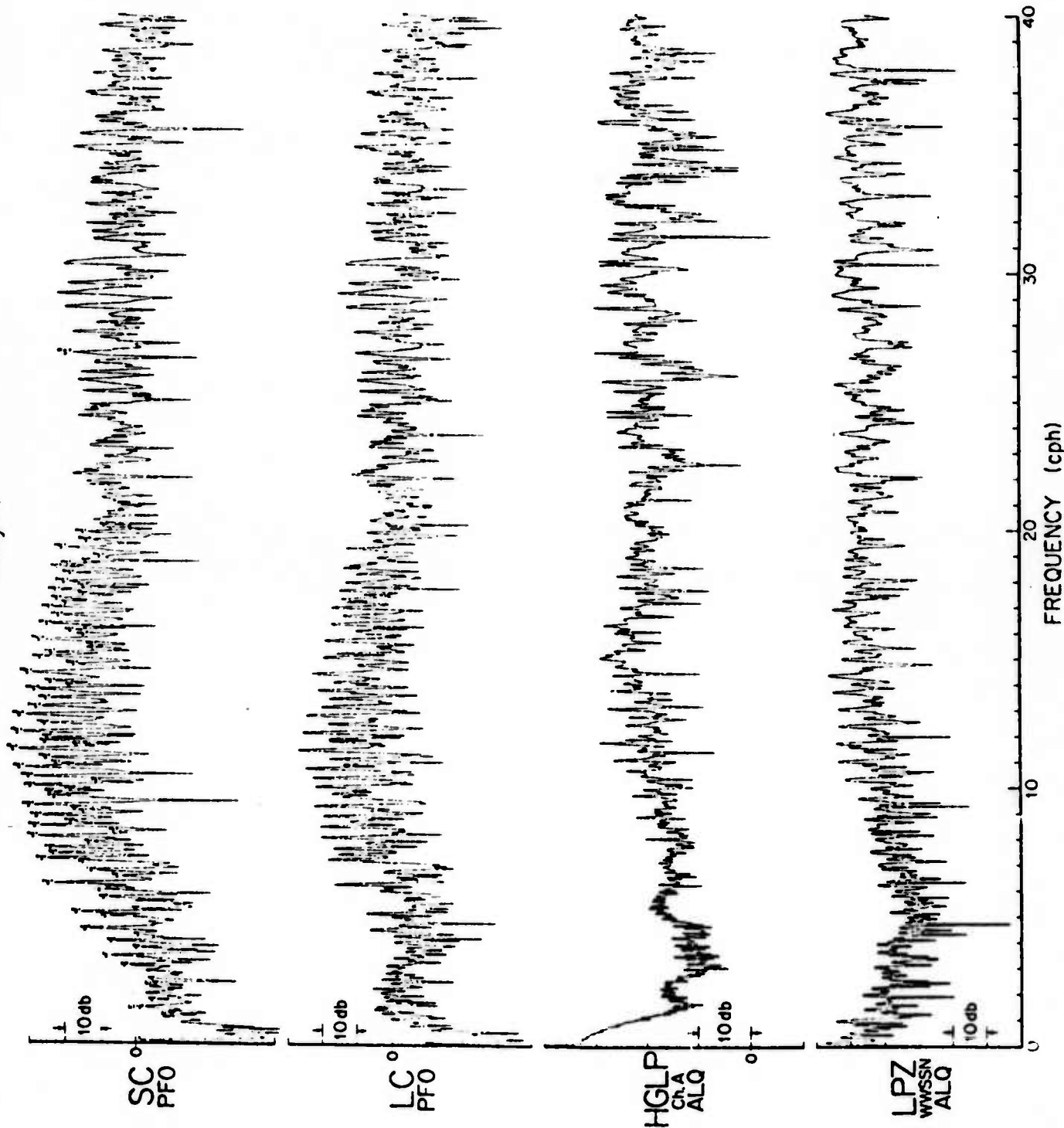
Figure A2

NORTH KOREA
Sept. 30, 1973 $m_b = 6.5$
(Day 2)

Figure A3

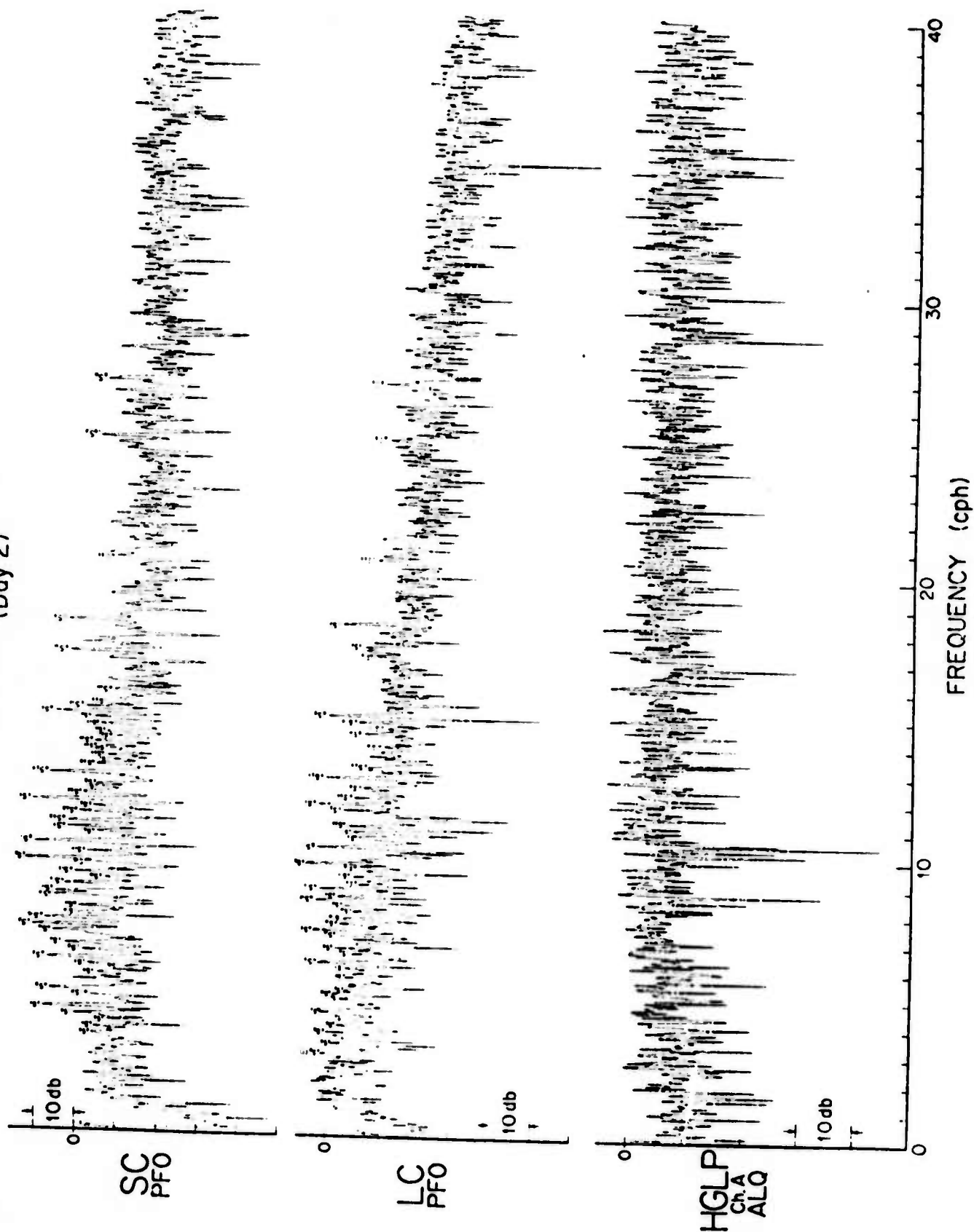SOLOMON ISLANDS
July 20, 1975
M = 7.8, NNA Tide

2000 sec

80 counts

START TIME 1200 UTC

'11
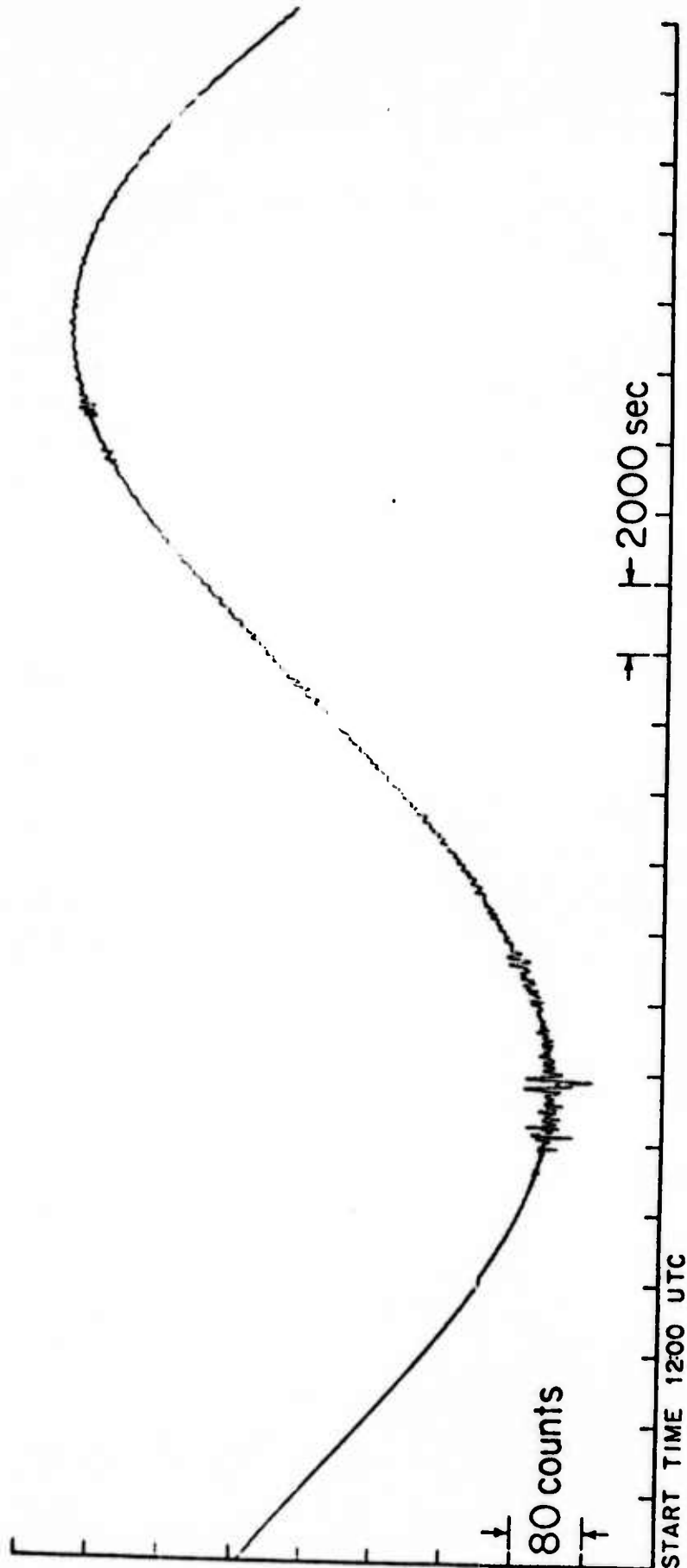
Figure A4

SOLOMON ISLANDS
July 20, 1975 at LPZ
(B channel at HGLP Z)

40 counts

2000 sec

START TIME 1200 UTC
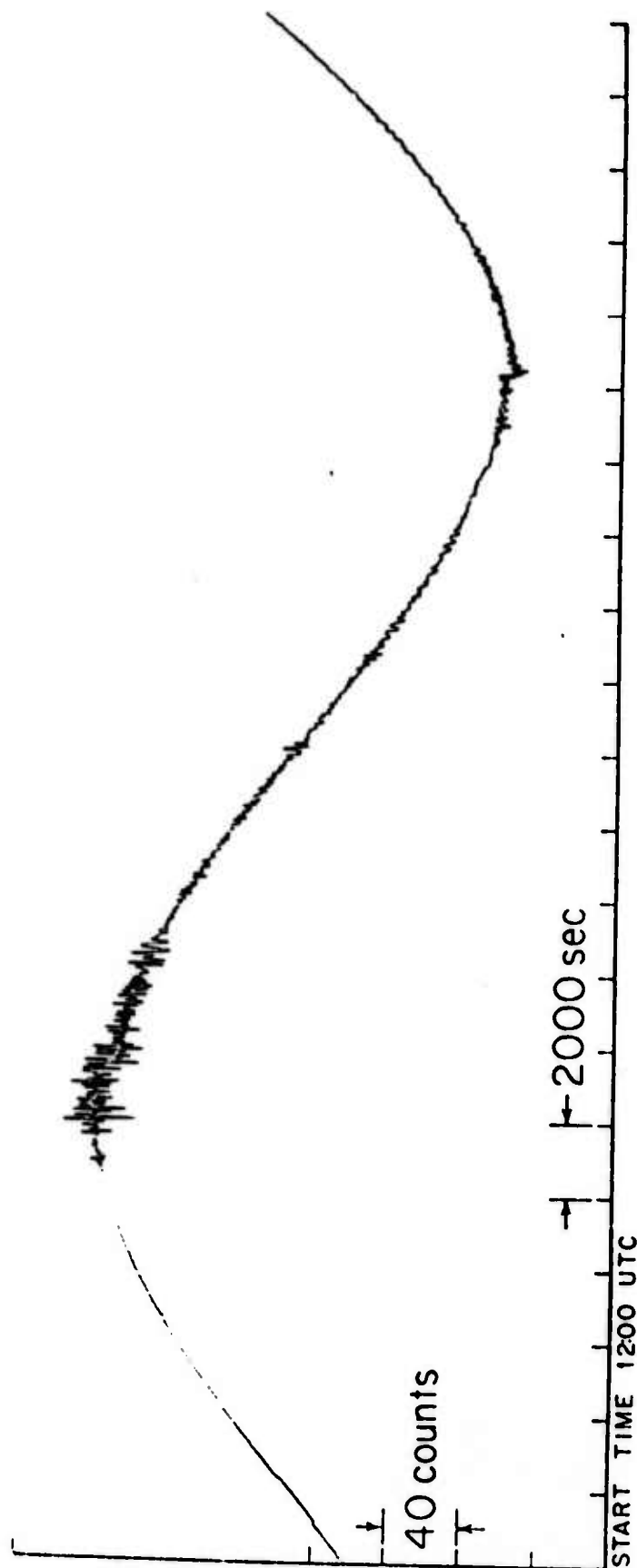
Figure A5

SOLOMON ISLANDS
July 20, 1975
M = 7.8 . NNA . x100 Mode Filter

├─2000 sec

410 counts

START TIME 1200 UTC
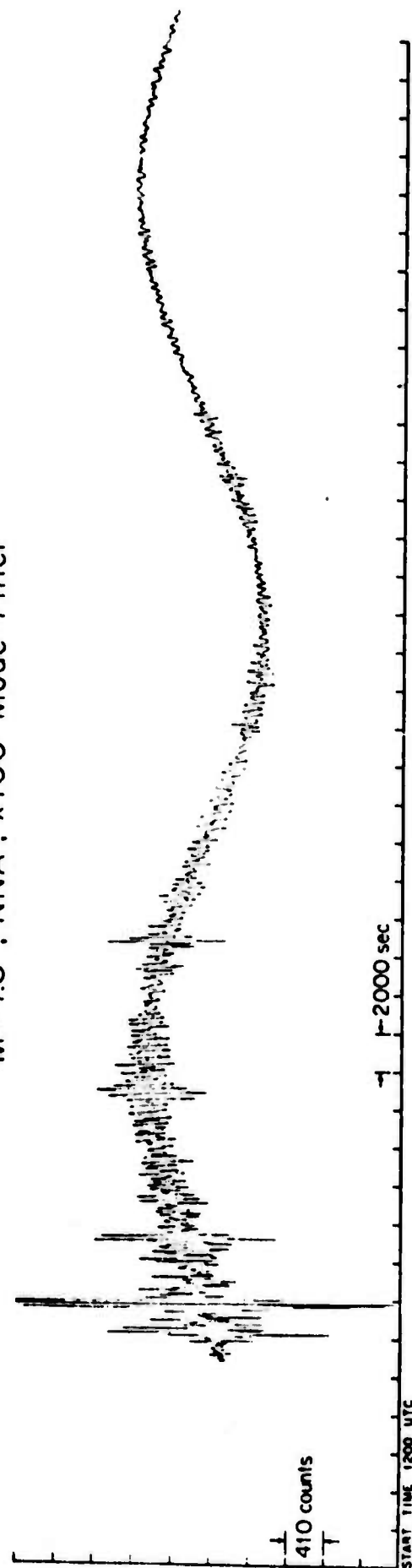
Figure A6

La Paz HGLP ch. B

FREQUENCY (mHz)

10db

Figure A7

14

Ñaña IDA LaCoste

Figure A8

15

Albuquerque SRO

16500 counts

1 hour
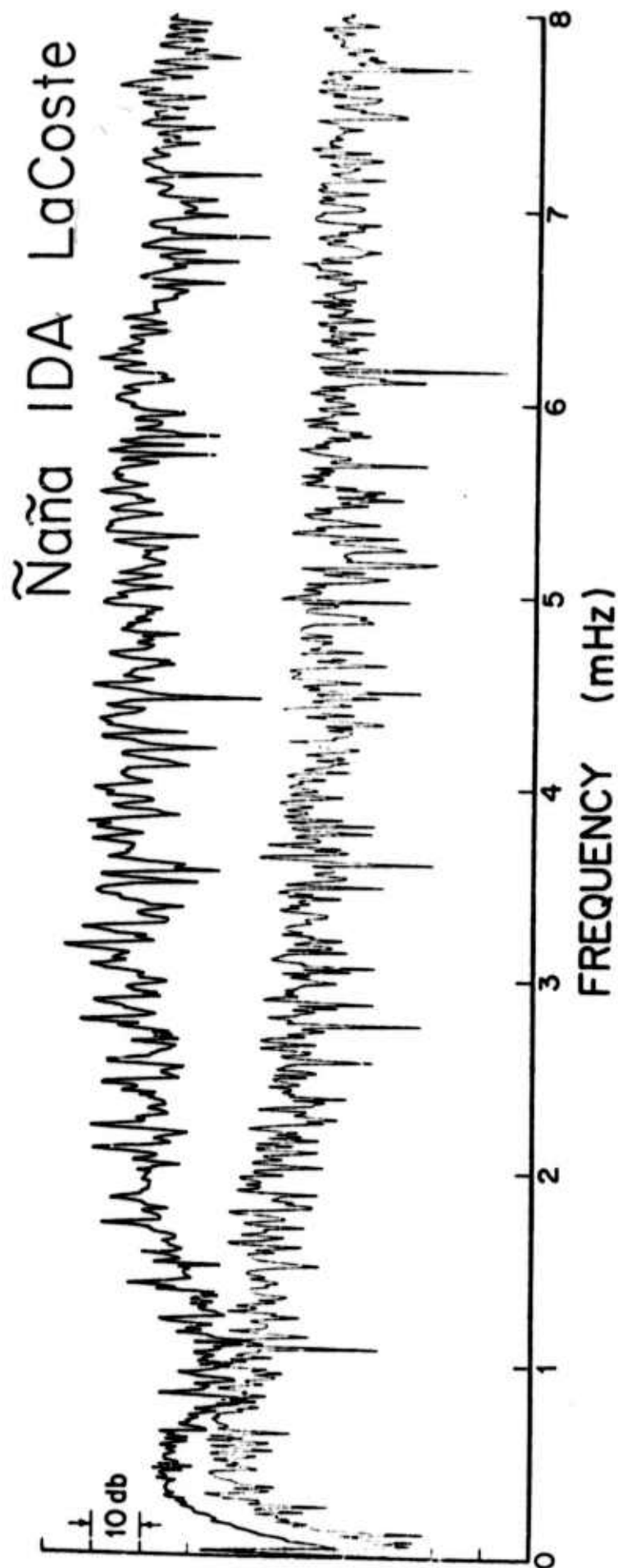
Figure A9

Figure A10

Albuquerque SRO

(R1 excluded)

FREQUENCY (mHz)

10 db

Figure A11

18
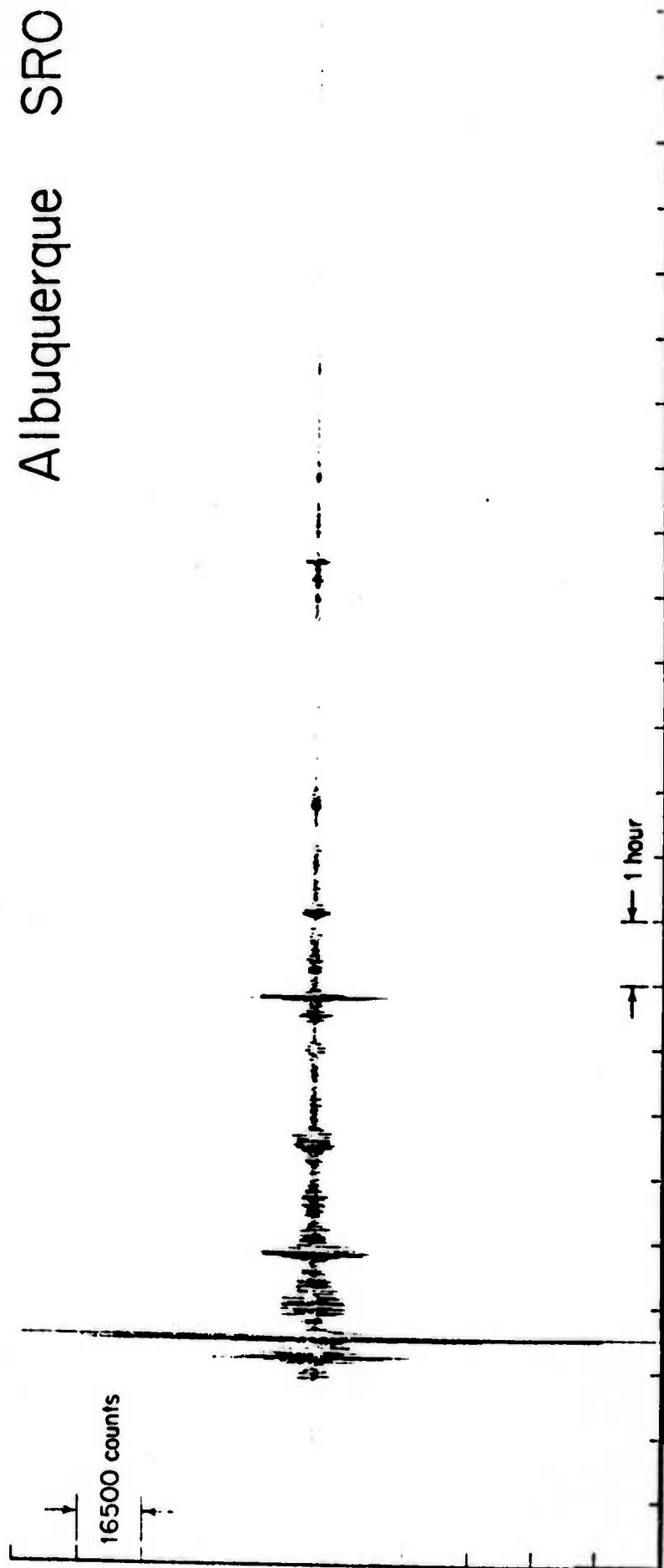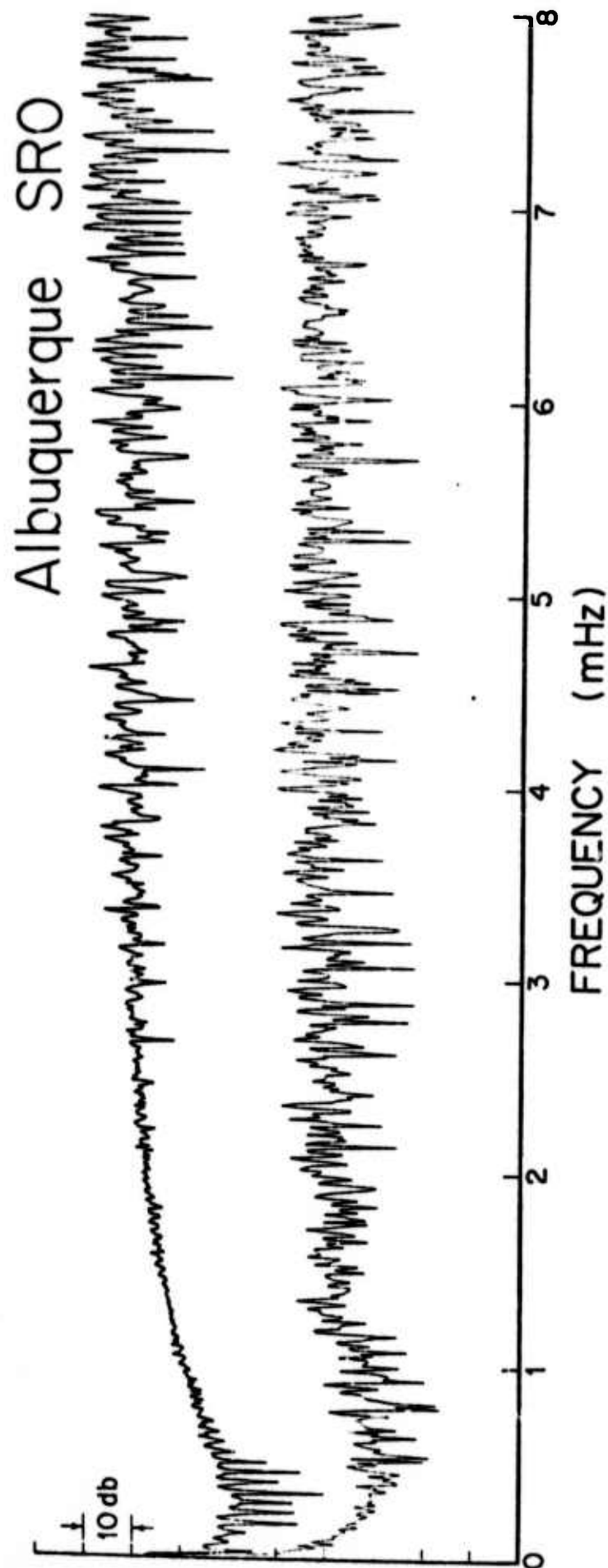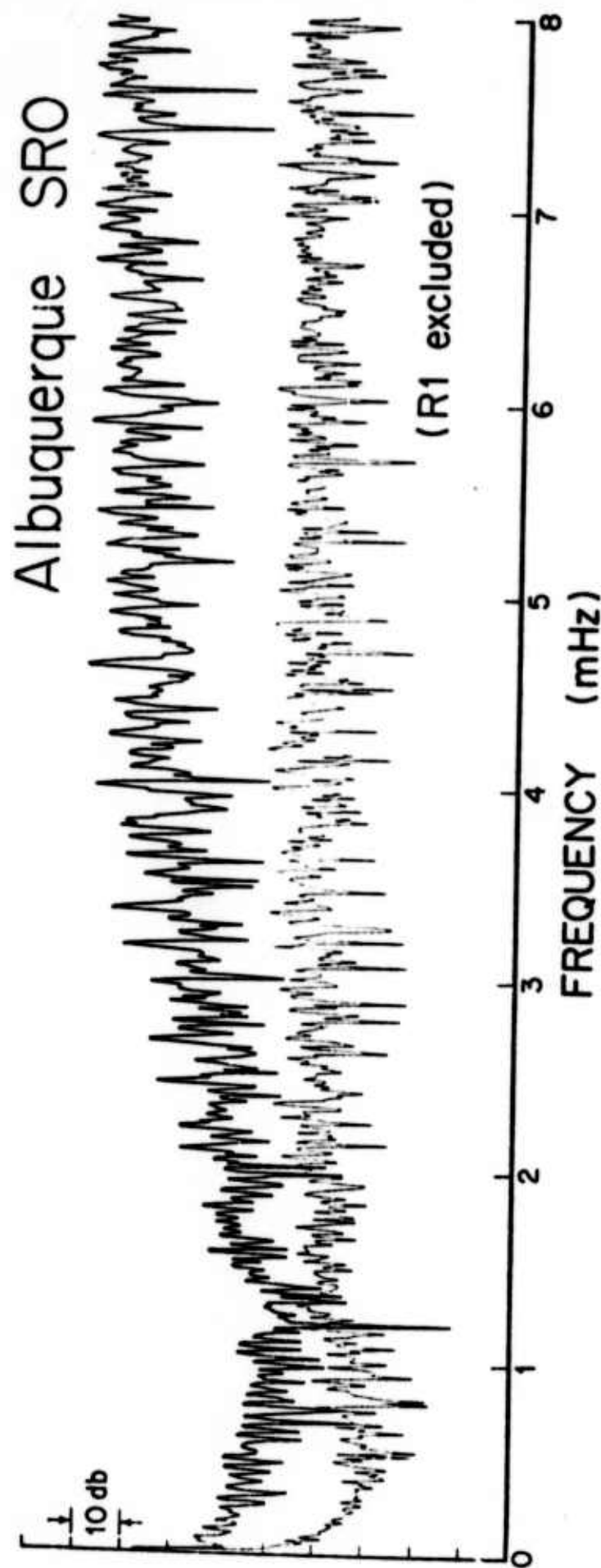
SOLOMON ISLANDS
July 1975 EARTHQUAKES
NNA, x100 Mode Filter
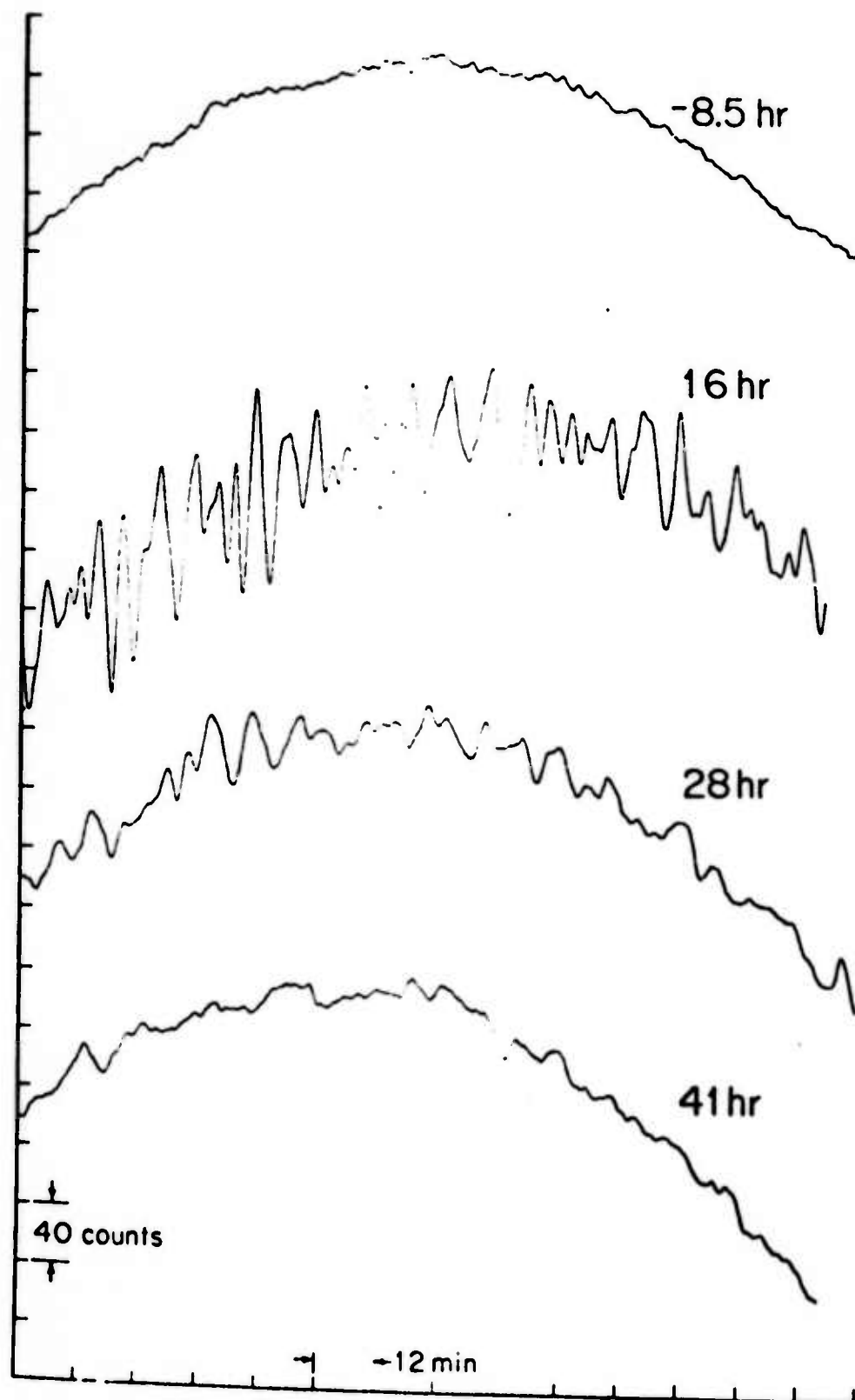
Figure A12

An Enhanced Deconvolution Procedure for Retrieving

the Seismic Moment Tensor from a Sparse Network

Freeman Gilbert and Ray Buland

Institute of Geophysics and Planetary Physics
Scripps Institution of Oceanography
University of California, San Diego
La Jolla, California 92093

Summary

In theory, a single horizontally polarized seismometer can be
used to find the six independent elements of the seismic moment tensor
of a buried point source, provided that the instrument is neither
longitudenally nor transversely polarized. Also, two vertically
polarized seismometers can be used, provided that the epicenter does
not lie on the great circle through the two instruments. These results
form the theoretical basis for a procedure for retrieving the source
mechanism from a sparse seismographic network.

B-i

Let the six independent elements of the seismic moment rate spectrum be $\underline{f}(\omega) = (f_1(\omega), \ldots, f_6(\omega))^T$ and suppose that P seismic spectra (records) $\underline{u}(\omega) = (u_1(\omega), \ldots, u_p(\omega))^T$ have been observed. The relationship between $\underline{u}(\omega)$ and $\underline{f}(\omega)$ is a linear one (Gilbert, 1971, 1973; Dziewonski and Gilbert, 1974; Gilbert and Dziewonski, 1975, hereafter referenced as M)

$$\underline{u}(\omega) = \underline{\underline{H}}(\omega) \cdot \underline{f}(\omega) \tag{1}$$

The $P \times 6$ matrix $\underline{\underline{H}}(\omega)$ is a functional of the mechanical structure of the Earth and can be regarded as the spectral transfer matrix or system function that relates output $\underline{u}(\omega)$ to input $\underline{f}(\omega)$. Let the $p^{\underline{th}}$ row of $\underline{\underline{H}}(\omega)$ be $\underline{h}^T_p(\omega)$.

The six-vector $\underline{h}_p(\omega)$ can be written as the sum of normal modes (M; 2.1.24, 2.1.28)

$$\underline{h}_p(\omega) = \sum_k \underline{A}_{kp} \, C_k(\omega) \, R_{kp}(\omega) \tag{2}$$

where A_{kp} specifies the excitation and amplitude of the $k^{\underline{th}}$ mode for the $p^{\underline{th}}$ record, C_k is the resonance function of the $k^{\underline{th}}$ mode, and R_{kp} represents the effect of truncation and the response of the $p^{\underline{th}}$ instrument. Each element of $\underline{h}_p(\omega)$ is the spectrum of a seismogram caused by a unit element of the moment rate tensor, a delta function in time. The observed seismogram at the $p^{\underline{th}}$ instrument is a linear

B-1

combination of the six seismograms $\underline{h}_p(\omega)$ and the six coefficients in the linear combination are the six elemr...s of $\underline{f}(\omega)$.

Suppose that our model of the Earth is good enough to permit us to ignore the difference between real and calculated $\underline{h}_p(\omega)$. Then we can seek to solve (1) for $\underline{f}(\omega)$. At low frequencies the spectral peaks in $\underline{h}_p(\omega)$ are sufficiently well separated to cause spectral gaps, frequencies where there is little or no information about $\underline{f}(\omega)$. However, it is generally believed that $\underline{f}(\omega)$ is a smooth function of ω at low frequencies, so smooth that it can be taken constant over a frequency band embracing many modes. Therefore, define set J of discrete frequencies ω_i

$$\omega_J - \delta\omega \le \omega_i \le \omega_J + \delta\omega \quad ; \quad i = i_J \, , \, i_J + 1 \, , \ldots \, , \, i_J + I - 1 \tag{3}$$

and replace $\underline{f}(\omega)$ by $\underline{f}(\omega_J)$. There are now $I \cdot P$ equations for the six-vector $\underline{f}$

$$\underline{u}_J = \underline{\underline{H}}_J \cdot \underline{f}(\omega_J) \tag{4}$$

and we solve (4) by applying the classical method of least squares

$$\underline{\underline{H}}_J^H \cdot \underline{u}_J = \underline{\underline{\mathscr{H}}}_J \cdot \underline{f}(\omega_J) \; ; \; \underline{\underline{\mathscr{H}}}_J = \underline{\underline{H}}_J^H \cdot \underline{\underline{H}}_J \tag{5}$$

where the superscript H denotes hermitean transpose.

In forming (5) we cross-correlate u_p with each element of $\underline{h}_p$ (multiply by $\underline{h}_p^H(\omega)$). This operation is conventionally termed matched filtering and is an operation to enhance the signal being sought. The

result is summed over the frequencies in set J to give (5). In order
to solve (5) for $\underline{f}$ we require that $\underset{\underline{\underline{\approx}}}{\mathcal{H}'}_J$ have rank-6 . Thus $I \cdot P \geq 6$
is a necessary condition. For a dense network, $P \gg 1$, I , the number
of discrete frequencies in set J , can be small. Alternatively if
$I \geq 6$ it appears that we can have $P = 1$ and still maintain rank-6
for $\underset{\underline{\underline{\approx}}}{\mathcal{H}}_J$. To explore this possibility we examine the eigenvalues of
$\underset{\underline{\underline{\approx}}}{\mathcal{H}}_J$. Without loss of generality we take $R_{kp}(\omega) = 1$.

Consider a single, vertically polarized accelerometer. In
epicentral spherical coordinates the location of the receiver is
(r , θ , ϕ) . An inspection of (M; 2.1.30) shows that the six vector
$\underline{A}_{kp}$ in (2) for vertical polarization (r-component) can be written

$$\underline{A} = (\underset{\underline{\underline{\approx}}}{\phi} \cdot \underline{S}) \, U(r) \tag{6}$$

where $\underset{\underline{\underline{\approx}}}{\phi}$ is a 6 x 4 matrix whose non-zero elements are

$$\phi_{11} = \phi_{22} = \phi_{32} = 1 \; , \; \phi_{23} = -\phi_{33} = \cos 2\phi \; , \; \phi_{44} = \cos\phi$$

$$\tag{7}$$

$$\phi_{54} = \sin\phi \; , \; \phi_{63} = 2 \sin 2\phi$$

and $\underline{S}$ is a 4-vector with components (M; 2.1.30)

$$S_1 = \epsilon_1^0 \, X_\ell^0 \; , \; S_2 = \epsilon_2^0 \, X_\ell^0 \; , \; S_3 = 2\epsilon_2^2 \, X_\ell^2 \; , \; S_4 = 2\epsilon_4^1 \, X_\ell^1 \tag{8}$$

Substituting (6) into (2) gives,

$$\underline{h}(\underline{r} , \omega) = \underline{\underline{\phi}} \cdot \underline{P}(\underline{r} , \omega) ; \underline{P}(\underline{r} , \omega) = \sum_k \underline{S}_k C_k(\omega) U_k(r) \qquad (9)$$

where $\underline{P}(\underline{r} , \omega)$ is a 4-vector. For $\underline{\underline{\mathscr{H}}}_J$ we have

$$\underline{\underline{\mathscr{H}}}_J = \underline{\underline{\phi}} \cdot \underline{\underline{\mathscr{P}}} \cdot \underline{\underline{\phi}}^T \qquad (10)$$

where

$$\underline{\underline{\mathscr{P}}} = \sum_i \underline{P}^*(\underline{r} , \omega_i) \underline{P}^T(\underline{r} , \omega_i) \qquad (11)$$

and the asterisk denotes complex conjugate. In (10) the 4 x 4 hermitean matrix $\underline{\underline{\mathscr{P}}}$ is limited to rank-4 and, therefore, so is $\underline{\underline{\mathscr{H}}}_J$. Consequently, the 6 x 6 hermitean matrix $\underline{\underline{\mathscr{H}}}_J$ is singular, and, not surprisingly, the moment rate tensor cannot be retrieved from the spectrum of a single, vertically polarized accelerometer. However, if I, the number of discrete frequencies in set J, is large enough ($I \geq 4$ is necessary) then $\underline{\underline{\mathscr{P}}}$ can have rank-4. We shall assume that $\underline{\underline{\mathscr{P}}}$ is rank-4.

Consider two, vertically polarized accelerometers with coordinates (θ_1 , ϕ_1) and (θ_2 , ϕ_2). In an obvious notation (10) becomes

$$\underline{\underline{\mathscr{H}}}_J = \underline{\underline{\phi}}_1 \cdot \underline{\underline{\mathscr{P}}}_1 \cdot \underline{\underline{\phi}}_1^T + \underline{\underline{\phi}}_2 \cdot \underline{\underline{\mathscr{P}}}_2 \cdot \underline{\underline{\phi}}_2^T \qquad (12)$$

If $\phi_1 = \phi_2$ then $\underline{\underline{\phi}}_1 = \underline{\underline{\phi}}_2$ and (11) becomes

$$\underline{\underline{\mathscr{H}}}_J = \underline{\underline{\phi}} \cdot (\underline{\underline{\mathscr{P}}}_1 + \underline{\underline{\mathscr{P}}}_2) \cdot \underline{\underline{\phi}}^T \qquad (13)$$

making $\underline{\underline{\mathscr{H}}}_J$ singular. Also, if $|\phi_1 - \phi_2| = \pi$, $\underline{\underline{\phi}}_1$ and $\underline{\underline{\phi}}_2$ are the same except for the sign of column 4. If we change the sign of column 4 and row 4 of $\underline{\underline{\mathscr{P}}}_2$ we have (13) again. Therefore, if the epicenter lies

on the great circle through the two vertical instruments, $\underline{\underline{\mathcal{H}}}_J$ is singular. Included here is the special case $\theta_1 = 0$, π or $\theta_2 = 0$, π. By a proper choice of coordinates we can always have $-\phi_2 = \phi_1 = \phi$ in (12). Assuming that $\underline{\underline{\mathcal{P}}}_1$ and $\underline{\underline{\mathcal{P}}}_2$ both have rank-4 we deal with the matrix $\underline{\underline{\phi}}(\phi) \cdot \underline{\underline{\phi}}^T(\phi) + \underline{\underline{\phi}}(-\phi) \cdot \underline{\underline{\phi}}^T(-\phi)$ which has rank-6 unless $\phi = 0$, $\pi/2$, π. Therefore, if the epicenter does not lie on the great circle through the two instruments, $\underline{\underline{\mathcal{H}}}_J$ is non-singular and (5) can be solved for $\underline{f}(\omega_J)$.

This result is important because it shows that a sparse global network of vertically polarized instruments can be used to retrieve the seismic moment rate tensor. Buland and Gilbert (1976) have shown that using ten WWSSN stations leads to a satisfactory result for $m_b = 7$.

To consider horizontally polarized instruments we must take into account toroidal as well as spheroidal modes. We introduce the 6 x 2 matrix $\underline{\underline{\Psi}}$ whose non-zero elements are

$$\Psi_{21} = -\Psi_{31} = \sin 2\phi \ , \ \Psi_{61} = -2\cos 2\phi \ , \ \Psi_{42} = \sin\phi \ , \ \Psi_{52} = -\cos\phi \qquad (14)$$

and the 2-vector $\underline{T}$ (M; 2.1.31)

$$T_1 = \epsilon_6^2 \, X_\ell^2 \qquad T_2 = 2\epsilon_5^1 \, X_\ell^1 \qquad (15)$$

In terms of $\underline{\underline{\Psi}}$ and $\underline{T}$, $\underline{A}$ in (M; 2.1.28) for toroidal modes is

$$\underline{A} = -\hat{\underline{\theta}} \csc \theta \, \partial_\phi \, (\underline{\underline{\Psi}} \cdot \underline{T}) W(r) + \hat{\underline{\phi}} \, \partial_\theta \, (\underline{\underline{\Psi}} \cdot \underline{T}) \, W(r) \tag{16}$$

and

$$\underline{h}_2(\underline{r}, \omega) = -\partial_\phi \underline{\underline{\Psi}} \cdot \sum_k \csc \theta \, \underline{T}_k C_k(\omega) W_k(r) = -\underline{\Psi}' \cdot \underline{Q} \csc \theta \tag{17}$$

$$\underline{h}_3(\underline{r}, \omega) = \underline{\underline{\Psi}} \cdot \sum_k \partial_\theta \, \underline{T}_k C_k(\omega) W_k(r) = \underline{\underline{\Psi}} \cdot \underline{Q}'$$

$\underline{h}_2$ and $\underline{h}_3$ for spheroidal modes are

$$\underline{h}_2(\underline{r}, \omega) = \underline{\underline{\phi}} \cdot \partial_\theta \underline{D} = \underline{\underline{\phi}} \cdot \underline{D}' \; ; \quad \underline{D}(\underline{r}, \omega) = \sum_k \underline{S}_k C_k(\omega) \, V_k(r) \tag{18}$$

$$\underline{h}_3(\underline{r}, \omega) = \partial_\phi \underline{\underline{\phi}} \cdot \underline{D} \csc \theta = \underline{\underline{\phi}}' \cdot \underline{D} \csc \theta$$

Thus the complete "synthetic seismograms" are

$$\underline{h}_2(\underline{r}, \omega) = \underline{\underline{\Omega}}_2 \cdot \underline{R}_2(\omega) \;, \quad \underline{\underline{\Omega}}_2 = \underline{\underline{\phi}} \oplus -\underline{\underline{\Psi}}' \;, \quad \underline{R}_2 = \underline{D}' \oplus \underline{Q} \csc \theta \tag{19}$$

$$\underline{h}_3(\underline{r}, \omega) = \underline{\underline{\Omega}}_3 \cdot \underline{R}_3(\omega) \;, \quad \underline{\underline{\Omega}}_3 = \underline{\underline{\phi}}' \oplus \underline{\underline{\Psi}} \;, \quad \underline{R}_3 = \csc \theta \, \underline{D} \oplus \underline{Q}'$$

where the 6 x 6 matrices $\underline{\underline{\Omega}}_2$ and $\underline{\underline{\Omega}}_3$ are functions only of ϕ and the 6-vectors $\underline{R}_2$ and $\underline{R}_3$ are functions of r, θ and ω. For both $\underline{\underline{\Omega}}_2$ and $\underline{\underline{\Omega}}_3$ the fifth column is proportional to the third and the sixth to the fourth. Also, columns 1 and 2 of $\underline{\underline{\Omega}}_3$ are zero. Thus $\underline{\underline{\Omega}}_2$ has rank-4 and $\underline{\underline{\Omega}}_3$ has rank-2. When we sum over set J to obtain $\underline{\underline{\mathscr{H}}}_J$ we use the 6 x 6 matrices

$$\underline{\underline{\mathscr{R}}}_{\beta\gamma} = \sum_i \underline{R}_{\beta}^{*}(\omega_i)\, \underline{R}_{\gamma}^{T}(\omega_i) \; ; \; \beta \,,\, \gamma = 2 \,,\, 3 \tag{20}$$

and we have $\underline{\underline{\mathscr{R}}}_{\beta\gamma}^{H} = \underline{\underline{\mathscr{R}}}_{\gamma\beta}$. We assume $\underline{\underline{\mathscr{R}}}_{\beta\gamma}$ to have rank-6. Although this assumption will be supported for ω-bands that include multiplets for several values of ℓ , $\underline{\underline{\mathscr{R}}}_{\beta\gamma}$ approaches singularity for large ℓ . This is a result of $\| \underline{D}' \| / \| \underline{D} \| = O(\ell)$ for large ℓ . The same is true for $\underline{Q}$. This means that $\underline{\underline{\mathscr{R}}}_{22}$ approaches rank-4 as an upper left 4×4 block, $\underline{\underline{\mathscr{R}}}_{33}$ approaches rank-2 as a lower right 2×2 block, and $\underline{\underline{\mathscr{R}}}_{23}$ approaches rank-2 as an upper right 4×2 block. Physically, this decomposition is a result of spheroidal modes dominating the θ-component and of toroidal modes dominating the ϕ-component for large ℓ .

We now consider a single, horizontally polarized instrument oriented at an angle α with respect to the $\hat{\underline{\theta}}$-vector. In terms of (19) and (20) $\underline{\underline{\mathscr{H}}}_J$ is

$$\underline{\underline{\mathscr{H}}}_J = \cos^2\alpha \; \underline{\Omega}_2 \cdot \underline{\underline{\mathscr{R}}}_{22} \cdot \underline{\Omega}_2^T + \cos\alpha \, \sin\alpha (\underline{\Omega}_2 \cdot \underline{\underline{\mathscr{R}}}_{23} \cdot \underline{\Omega}_3^T +$$

$$+ \underline{\Omega}_3 \cdot \underline{\underline{\mathscr{R}}}_{32} \cdot \underline{\Omega}_2^T) + \sin^2\alpha \; \underline{\Omega}_3 \cdot \underline{\underline{\mathscr{R}}}_{33} \cdot \underline{\Omega}_3^T \tag{21}$$

In general, $\underline{\underline{\mathscr{H}}}_J$ will be non-singular. However, if $\alpha = 0$, longitudenal polarization , or $\pi/2$, transverse polarization, $\underline{\underline{\mathscr{H}}}_J$ will be singular because $\underline{\Omega}_2$ and $\underline{\Omega}_3$ are singular. Also, the matrices $\underline{\underline{\mathscr{R}}}_{\beta\gamma}$ have

rank-2 for $\theta = 0 , \pi$. This means that a source directly beneath
the receiver or its antipode cannot be retrieved. Otherwise, the
moment rate tensor can be retrieved from a *single*, horizontally
polarized instrument. As in the previous example, for two vertical
instruments, it is necessary to sum over an ω-band containing multiplets
for several values of ℓ , in order that $\underline{\underline{\mathcal{R}}}_{\beta\gamma}$ have full rank, and it is
assumed that $\underline{f}(\omega)$ is nearly constant in each ω-band. This result
remains true for large ℓ even though $\underline{\underline{\mathcal{R}}}_{\beta\gamma}$ becomes singular. Since
$\underline{\underline{\mathcal{R}}}_{22}$ becomes an upper left 4 x 4 block we can replace $\underline{\underline{\Omega}}_2$ by $\underline{\underline{\Phi}}$ in
(21). Similarly, we can replace $\underline{\underline{\Omega}}_3$ by $\underline{\underline{\Psi}}$. Let

$$\underline{\underline{\mathcal{R}}} = \cos^2\alpha\, \underline{\underline{\mathcal{R}}}_{22} + \sin^2\alpha\, \underline{\underline{\mathcal{R}}}_{33} + \cos\alpha\,\sin\alpha\, (\underline{\underline{\mathcal{R}}}_{23} + \underline{\underline{\mathcal{R}}}_{32})$$

(22)

$$\underline{\underline{\Omega}} = \underline{\underline{\Phi}} \oplus \underline{\underline{\Psi}}$$

For large ℓ (21) becomes

$$\underline{\underline{\mathcal{H}}}_J = \underline{\underline{\Omega}} \cdot \underline{\underline{\mathcal{R}}} \cdot \underline{\underline{\Omega}}^T$$

(24)

In (24) we assume that I , the number of discrete frequencies in set J ,
is large enough to make $\underline{\underline{\mathcal{R}}}$ have rank-6 . Since det $\underline{\underline{\Omega}} \neq 0$ (actually
det $\underline{\underline{\Omega}} = 8$) we see that $\underline{\underline{\mathcal{H}}}_J$ has rank-6 . Thus, even at short periods,
the moment rate tensor can be retrieved from a single horizontal
instrument unless $\alpha = 0 , \pi/2$ or $\theta = 0 , \pi$.

In practice, a seismographic station has two horizontal instruments,
in which case it is clear that the moment rate tensor can be retrieved.

Moreover, a standard installation, consisting of one vertical and two horizontal instruments certainly enables the retrieval of the moment rate tensor. Here, the only exclusion is $\vartheta = 0$, π .

The foregoing examples demonstrate theoretically that, except in special circumstances, the moment rate tensor of a buried point source can be retrieved from the spectra of *two* vertical accelerometers or from the spectrum of *one* horizontal accelerometer. From these theoretical results we can easily infer that a *network* of a small number of instruments can be used to retrieve source mechanisms on a routine basis. The ability to achieve such retrievals makes possible some interesting research projects.

The method presented here is an extension of the concept of matched filtering (see, for example, Robinson, 1967, pp. 259-264). The matched filters, $\underline{h}(\underline{r}$, $\omega)$ in (2), are the best linear filters in that they maximize the signal/noise ratio. For Gaussian noise they are optimum.

Although we have obtained $\underline{h}(\underline{r}$, $\omega)$ in (2) by summing normal mode multiplets, it should be emphasized that the method of retrieval is independent of the procedure used to obtain $\underline{h}(\underline{r}$, $\omega)$. Any procedure for generating synthetic seismograms can be used to obtain $\underline{h}(\underline{r}$, $\omega)$. Therefore, matched filtering for the seismic moment tensor can be done globally, regionally or locally, depending on the magnitude of the seismic source and the configuration of the network.

References

Buland, R. & Gilbert, F., 1976. Matched filtering for the seismic
moment tensor, *Geophys. Res. Lttrs.*, submitted.

Dziewonski, A. M. & Gilbert, F., 1974. Temporal variation of the
seismic moment tensor and the evidence of precursive
compression for two deep earthquakes, *Nature*, 247, 185-188.

Gilbert, F., 1971. Excitation of the normal modes of the Earth by
earthquake sources, *Geophys. J. R. astr. Soc.*, 21, 223-226.

Gilbert, F., 1973. Derviation of source parameters from low-frequency
spectra, *Phil. Trans. R. Soc. (London)* A, 274 , 369-371.

Gilbert, F. & Dziewonski, A. M., 1975. An application of normal
mode theory to the retrieval of structural parameters
and source mechanisms from seismic spectra, *Phil. Trans. R. Soc.
(London)* A, 278, 187-269.

Robinson, E. R., 1967. *Statistical Communication and Detection*,
Hafner, New York.

MATCHED FILTERING FOR THE SEISMIC MOMENT TENSOR

Ray Buland and Freeman Gilbert
Institute of Geophysics and Planetary Physics
Scripps Institution of Oceanography
University of California, San Diego
La Jolla, California   92093

C-i

ABSTRACT

By a process of matched filtering it is possible to deconvolve
a small number of acceleration or strain records for the moment rate
tensor of a seismic source. Theoretically, one horizontal accelerometer
(or strain meter) or two vertical accelerometers is sufficient. Practically,
five to ten records can be shown to suffice. Specifically, the mechanism
of the Colombian event of July 31, 1970 can be retrieved from a sparse
network of ten WWSSN vertical instruments. With currently available
instrumentation it should be possible to discriminate unambiguously
between an earthquake and an explosion larger than magnitude 6 at
teleseismic distances. Improved, digitally recorded networks can
lead to a decrease in the threshold of discrimination.

We consider the moment rate tensor for a buried point source. The problem of retrieving the elements of the moment rate tensor (Gilbert and Dziewonski, 1975, Section 2.3; hereafter referenced as M) has been discussed by Dziewonski and Gilbert (1974). Their method, an extension of a suggestion of Gilbert (1973), depends on the orthogonality relations for the spherical harmonics, and implies a dense global array of receivers. The paucity of first quality long period instruments motivates a search for a method requiring only a sparse network.

Following (M; 2.1.17), let the Fourier transform of the moment rate tensor, $\underline{\underline{M}}(\omega)$, be written as the six-vector, $\underline{f}(\omega)$. Then the Fourier transform of the $p^{\underline{th}}$ displacement (or strain, etc.) record, due to $\underline{f}(\omega)$, at the $i^{\underline{th}}$ frequency, $U_p(\omega_i)$, may be written as a sum of normal nodes (M; 2.1.24, 2.1.28).

$$U_p(\omega_i) = \sum_k \underline{A}_{kp}^T \cdot \underline{f}(\omega_i) \, C_k(\omega_i) \, R_p(\omega_i) \tag{1}$$

Where $\underline{A}_{kp}$ specifies the excitation and amplitude of the $k^{\underline{th}}$ mode at the $p^{\underline{th}}$ instrument; C_k is the resonance function of the $k^{\underline{th}}$

normal mode; and R_p is the instrument response and truncation effect at the pth instrument. Define matched filters

$$\underline{h}_p(\omega_i) = \sum_k \underline{A}_{kp} C_k(\omega_i) R_p(\omega_i) \quad . \tag{2}$$

For P records we have P equations in six unknowns; $f_1, \ldots, f_6$

$$\underline{U}(\omega_i) = \underline{\underline{H}}(\omega_i) \cdot \underline{f}(\omega_i) \tag{3}$$

where the pth element of $\underline{U}(\omega_i)$ is $U_p(\omega_i)$ and the pth row of $\underline{\underline{H}}(\omega_i)$ is $\underline{h}_p^T(\omega_i)$. Clearly, if $P \geq 6$ we can solve (3) by least squares for $\underline{f}(\omega_i)$, the moment rate tensor at frequency point ω_i .

Because of ground and instrumental noise, and splitting and uncertainties in Q structure, it is unlikely that $\underline{f}(\omega_i)$ will be well determined for a small number of stations. However, from M(Figures 6 and 7) we suspect that $\underline{f}$ is a smooth function of frequency. Therefore, define set J of discrete frequencies ω_i such that $\omega_J - \delta\omega \leq \omega_i \leq \omega_J + \delta\omega$, $i = 1, 2, \ldots, I$. Assume that $\underline{f}(\omega_J) = \underline{f}(\omega_1) = \ldots = \underline{f}(\omega_I)$. We now have $P \cdot I$ equations in six unknowns

$$\underline{U}_J = \underline{\underline{H}}_J \cdot \underline{f}(\omega_J) \quad . \tag{4}$$

As I , the number of frequency points in set J , may be large there appears to be no reason that P cannot be unity. To explore

the limits of the method we have examined the eigenvalues of the normal matrix

$$\underline{\mathscr{H}}_J = \underline{H}_J^* \cdot \underline{H}_J \tag{5}$$

where the superscript $*$ means hermitean transpose. A detailed analysis is beyond the scope of this letter and will appear elsewhere. The results will be stated without proof. Two vertical accelerometers (not lying on a great circle through the epicenter) or one horizontal accelerometer (not longitudinally or transversely polarized) give full rank to $\underline{\mathscr{H}}_J$. Practically, synthetic numerical experiments indicate that a minimum of five to ten stations is satisfactory.

For large P we examine the relationship between the above method and the method described in (M;2.3). For simplicity assume $P_p(\omega) \equiv 1$. Multiplying equation (4) by $\underline{H}_J^*$ (explicity forming the normal equations) and expanding the sums

$$\sum_{i,p} \left[\sum_k \underline{A}_{kp} \, c_k^*(\omega_i) \right] U_p(\omega_i)$$

$$= \left\{ \sum_{i,p} \left[\sum_k \underline{A}_{kp} \, c_k^*(\omega_i) \right] \left[\sum_j \underline{A}_{jp}^T \, c_j(\omega_i) \right] \right\} \cdot \underline{f}(\omega_J) \, . \tag{6}$$

Rearrange equation (6)

$$\sum_{p,k} \left[\sum_i c_k^*(\omega_i) \, U_p(\omega_i) \right] \underline{A}_{kp}$$

$$= \left\{ \sum_{k,j} \left[\sum_i c_k^*(\omega_i) \, c_j(\omega_i) \right] \left[\sum_p \underline{A}_{kp} \, \underline{A}_{jp}^T \right] \right\} \cdot \underline{f}(\omega_J) \tag{7}$$

and define

$$I_k(v) \equiv \int\limits_{\omega_J-\delta\omega}^{\omega_J+\delta\omega} C_k^*(\omega) \ v \ (\omega)d\omega \approx \sum_i C_k^*(\omega_i) \ v \ (\omega_i) \ . \tag{8}$$

Using the orthogonality relation (M; 2.3.2) among modes (valid for a dense array) rewrite equation (7) as

$$\sum_{p,k} I_k(U_p) \ \underline{A}_{kp} = \left\{ \sum_{p,k} I_k(C_k) \ \underline{A}_{kp} \ \underline{A}_{kp}^T \right\} \cdot \underline{f}(\omega_J) \ . \tag{9}$$

Equation (9) differs from M; 2.3.2-2.3.10 only in the definition of $I(v)$. However, equation (8) shares with its counterpart (M; 2.3.7) the insensitivity to Q gained by integrating across the resonance function. The fundamental difference between matched filtering (equation (6)) and stacking (equation (9) and (M;2.3.8)) is that matched filtering includes all the cross terms among modes (does not depend on the orthogonality relation).

The method presented here employs an extension of the concept of matched filtering (see, for example, Robinson, 1967, pp. 259-264). The matched filters, $\underline{h}_p(\omega_i)$, in (2), are the best linear filters in that they maximize the signal/noise ratio. Intuitively, we remove noise and scattered energy from a record by forcing our prejudice on each record that it be a linear combination of six synthetic records. The data are then frequency averaged over set J (sum on i in equation (6)) to reduce sensitivity to splitting and Q structure and to stabilize $\underline{\mathcal{H}}_J$. Spatial averaging (sum on p in equation (6)) further stabilizes the system. Finally, the P records are deconvolved for $\underline{f}(\omega_J)$ by inverting $\underline{\mathcal{H}}_J$.

As an example of the method we have plotted (figure 1) the raw M_{rr} component derived by matched filtering from a ten record subset (vertical first day data from stations GUA, JER, KIP, CHG, GIE, GDH, PTO, NAI, NAT, KBL) of the Colombian data set (M; Table 1) and M_{rr} redrawn from (M, Figure 6). The agreement is apparent and, considering the quality of WWSSN data at very long periods, acceptable. Figure 1 emphasizes the demand for quality data if P is to be small.

Given the availability of quality, long period, digital data, matched filtering provides a method for routinely and rapidly determining the complete long period source function of any event larger than about magnitude 6 at teleseismic distances. This should greatly facilitate studies of stress-release mechanisms. Furthermore, the implications for seismic discrimination are promising. Having calculated the complete long period source function of an event, the discrimination between an earthquake and an explosion is entirely unambiguous.

Although we have obtained $h_p(\omega_i)$ by summing normal mode multiplets, it should be emphasized that the method of retrieval is independent of the procedure used to obtain the matched filters. Any procedure for generating synthetic seismograms can be used. Therefore, matched filtering for the seismic moment tensor can be done globally, regionally or locally, depending on the magnitude of the seismic source and the configuration of the network.

Acknowledgements

REFERENCES

Dziewonski, A. M. and Gilbert, F. 1974. Temporal variation of the seismic moment tensor and the evidence of precursive compression for two deep earthquakes, *Nature*, **247**, 185-188.

Gilbert, F. 1973. Derivation of source parameters from low-frequency spectra, *Phil. Trans. R. Soc. Lond. A*, **274**, 369-371.

Gilbert, F. and Dziewonski, A. M. 1975. An application of normal mode theory to the retrieval of structural parameters and source mechanisms from seismic spectra, *Phil. Trans. R. Soc. Lond. A*, **278**, 187-269.

Robinson, E. R. 1967. *Statistical Communication and Detection*, Hafner, New York.

CAPTION

Figure 1. The real and imaginary parts of M_{rr} in dyne-cm/10^{27} . Triangles are redrawn from (M; Figure 6). Squares are calculated by matched filtering from 10 stations.
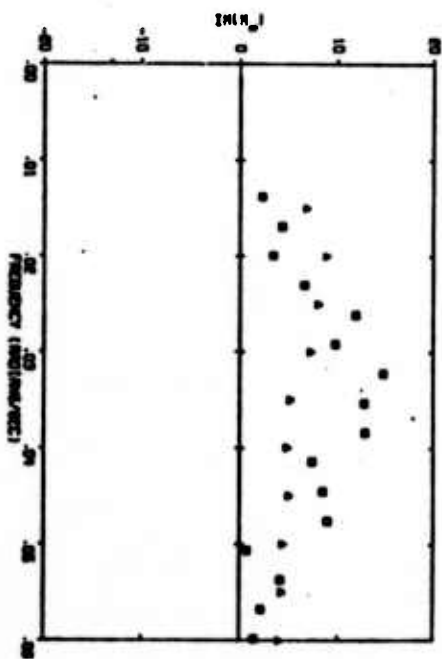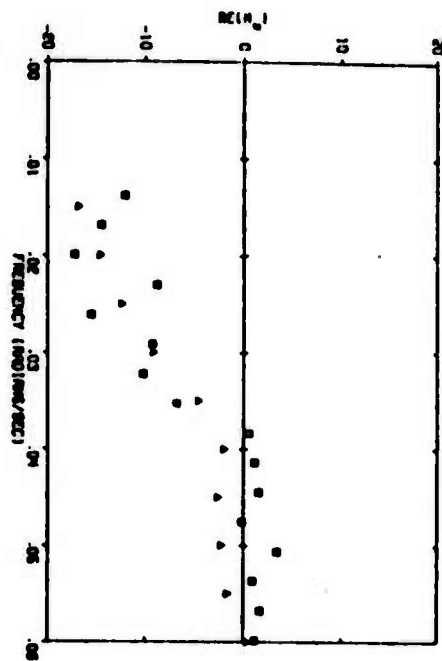
C-8

The Theoretical Basis for the Rapid and Accurate Computation

of Normal Mode Eigenfrequencies and Eigenfunctions

R. P. Buland and F. Gilbert

NOTE: Computational procedures have been developed for the
CDC 7600 at the Lawrence Berkeley Laboratory of the University
of California.

D1

Introduction

Recent progress in the application of normal mode theory in seismology has made it necessary to develop a practical and accurate scheme for the computation of the high frequency elastic-gravitational free oscillations of a radially symmetric, non-rotating, self gravitating, perfectly elastic earth model. The scheme developed is based on the classical variational approach and on recent advances in the solution of the algebraic eigenvalue problem for large banded systems of the form $(A - \lambda B)\underline{u} = \underline{0}$.

Raleigh-Ritz Procedure

By Raleigh's principle the eigenfunctions of an earth model are extremal solutions of the energy balance equation:

$$\omega^2 \int_0^a \mathcal{T}(r) r^2 dr - \int_0^a \mathcal{V}(r) r^2 dr = 0 \tag{1}$$

where $\omega^2 \mathcal{T}$ is the kinetic energy density per unit volume as a function of radius, $\mathcal{V}$ the corresponding potential energy density, ω the angular frequency, and a the radius of the earth (Pekeris and Jarosch, 1958, develop eq. 1 in terms of the radial scalars of an eigenfunction). Therefore, approximate eigenfunctions and eigenvalues may be computed from eq. 1 by a Raleigh-Ritz procedure. Let us represent the radial part of the eigenfunction $s(r)$ as a linear combination of N test functions $\zeta_i(r)$ each satisfying the boundary conditions.

$$s(r) \sim \overline{s}(r) = \sum_{i=1}^{N} b_i \zeta_i(r) \qquad (2)$$

substituting eq. 2 into eq. 1 results in a matrix eigenvalue problem:

$$A(\omega)\underline{b} = (\omega^2 T - V)\underline{b} = \underline{0} \qquad (3)$$

with the following properties:

1) Each eigenvector $\underline{b}$ represents a projection of eigen-function s onto the space spanned by the ζ_i's .

2) ω^2 is an upper bound to the squared eigenfrequency associated with eigenfunction s .

3) Each sucessive eigenvector $\underline{b}$ represents a higher radial order (overtone) of the same angular order. Each angular order is represented by a different matrix equation.

4) If the error between s and the projection of s onto the ζ_i's is $O(\alpha)$ then the error between ω^2 and the squared eigenfrequency associated with s is $O(\alpha^2)$.

Test Functions

For computational speed it is desirable that the test functions be economical to compute, that the number of test functions, N , be as small as is consistent with an accurate representation of s , and that each test function overlap only a small number of other test functions, i.e., the matrices T and V be banded (Courant, 1943). Further, we

demand that $\bar{s}$ be continuous and desire that $\partial_r \bar{s}(r)$ be continuous also except at first order discontinuities, where the usual boundary conditions apply. These requirements dictate the use of the basis functions for piecewise cubic Hermite interpolation as test functions (Birkhoff *et al.*, 1966).

Computational Philosophy

In order not to discard any precision unnecessarily it has been found desirable to adhere rigidly to an all pervading philosophy. As is common practice our models are specified at discrete points of an unequally spaced grid:

$$\nu : 0 = y_1 < y_2 < \cdots < y_M = a .$$

Each of the model parameters-- $\rho(r)$, $\mu(r)$, or $\lambda(r)$ --is defined to be the cubic spline interpolation of the parameter specified on grid ν . Similarly, the eigenfunctions are calculated on grid:

$$\pi : 0 = x_1 < x_2 < \cdots < x_N = a .$$

Due to the choice of test functions each eigenfunction must be defined as the Hermite cubic spline interpolation of the eigenfunction on grid π .

It has been found necessary to perform the integrals quite precisely. Our philosophy has been to sacrifice a little speed (since they need only be done once per model) and do the integrals exactly. Therefore, all integration has been performed interval by interval $(x_{i-1} \leq x \leq x_i$, $i = 2$, 3 , $\cdots$, N) by means of a low order

Gauss-Legendre quadrature. The integrals are thus both rapidly computed and numerically stable as well as mathematically exact. It has also been our philosophy to use no less than 6 nodes (12 degrees of freedom per radial scalar) per radial wavelength at the highest frequency of interest (G. Frazier, personal communication).

The Detailed Test Functions

Define basis functions

$$\eta_0(x) = \begin{cases} 2x^3 - 3x^2 + 1 & 0 \le x \le 1 \\ -2x^3 - 3x^2 + 1 & -1 \le x < 0 \\ 0 & \text{otherwise} \end{cases}$$

$$\psi_0(x) = \begin{cases} x^3 - 2x^2 + x & 0 \le x \le 1 \\ x^3 + 2x^2 + x & -1 \le x < 0 \\ 0 & \text{otherwise} \end{cases}$$

(4)

η_0 and ψ_0 are simply designed to be piecewise cubic, continuously differentiable functions with properties given in Table 1. The test functions are then defined by:

$$\eta_i(x) = \begin{cases} \eta_0\left(\dfrac{x - x_i}{x_{i+1} - x_i}\right) & x_i \le x \le x_{i+1} \\ \eta_0\left(\dfrac{x - x_i}{x_i - x_{i-1}}\right) & x_{i-1} \le x < x_i \\ 0 & \text{otherwise} \end{cases}$$

(5)

$$\psi_i(x) = \begin{cases} (x_{i+1} - x_i)\,\psi_0\left(\dfrac{x - x_i}{x_{i+1} - x_i}\right) & x_i \le x \le x_{i+1} \\ (x_i - x_{i-1})\,\psi_0\left(\dfrac{x - x_i}{x_i - x_{i-1}}\right) & x_{i-1} \le x < x_i \\ 0 & \text{otherwise} \end{cases}$$

Representation of the Eigenfunctions

Let us represent a toroidal free oscillation as:

$$_n\underline{\tau}_\ell^m(\underline{r},t) = \left[-_nW_\ell(r)\; \hat{r} \times \vec{\nabla}_1 Y_\ell^m(\theta,\phi)\right] e^{i\,_n\omega_\ell^m t}$$

$$_nW_\ell(r) \sim \sum_{i=1}^{N} \left[w_i^{(1)}\eta_i(r) + w_i^{(2)}\psi_i(r)\right] \quad .$$

(6)

Eq. 6 yields a matrix system with 2 degrees of freedom per node or $2N \times 2N$ matrices with half bandwidth 4 . Of course, for a model with zero viscosity in the outer core, the model need only include the mantle for this case.

Let us represent spheroidal free oscillations as:

$$_n\underline{\sigma}_\ell^m(\underline{r},t) = \left[\hat{r}\,_nU_\ell(r)Y_\ell^m(\theta,\phi) + \,_nV_\ell(r)\vec{\nabla}_1 Y_\ell^m(\theta,\phi)\right] e^{i\,_n\omega_\ell^m t}$$

$$_nU_\ell(r) \sim \sum_{i=1}^{N} \left[u_i^{(1)}\eta_i(r) + u_i^{(2)}\psi_i(r)\right]$$

(7)

$$_nV_\ell(r) \sim \sum_{i=1}^{N} \left[v_i^{(1)}\eta_i(r) + v_i^{(2)}\psi_i(r)\right]$$

coupled with the perturbation of the gravitational potential:

$$_n\gamma_\ell^m(\underline{r},t) = \left[\hat{r}\,_nP_\ell(r)Y_\ell^m(\theta,\phi)\right] e^{i\,_n\omega_\ell^m t}$$

$$_nP_\ell(r) \sim \sum_{i=1}^{N} \left[p_i^{(1)}\eta_i(r) + p_i^{(2)}\psi_i(r)\right] \quad .$$

(8)

Eq. 7 alone yields a matrix system with 4 degrees of freedom per node or
4N x 4N matrices with half bandwidth 8 . Eq. 7 coupled with eq. 8 yields
a 6N x 6N matrix system with half bandwidth 12 .

Boundary Conditions

Before the matrix eigenvalue problem in eq. 3 can yield valid
approximations to the eigenfrequencies and eigenfunctions of an earth
model, all boundary conditions must be satisfied. Rather than introduce
constraint equations with undetermined Lagrange multipliers (which
increases the size of the matrices) we have chosen explicitly to match
the boundary conditions by making linear combinations of the rows and
columns (and reducing the rank) of the matrices. Therefore, upon
entrance into the eigenvalue procedure all boundary conditions are
automatically and exactly satisfied.

Finding the Eigenvalues and Eigenvectors

By using the Sturm count (number of eigenvalues of eq. 3
larger than ω^2) and det $[A(\omega)]$, all eigenvalues in a given frequency
band may be quickly found to machine precision by bisection and linear
interpolation (Martin and Wilkinson, 1967; Peters and Wilkinson, 1969).
Even though each calculation of the determinant and Sturm count of
eq. 3 requires a new decomposition of the matrix $A(\omega)$, it is possible
to take advantage of the bandwidth of the system. Without the
small bandwidth of $A(\omega)$ the problem would be hopelessly expensive.
Once the eigenvalue is known the eigenvector may be found by inverse
iteration (Wilkinson, 1965, p 628-629).

If the half bandwidth is m , then the number of operations needed
to find each eigenvalue goes as Nm^2 .   The amount of computation is
independent of n, ℓ, ω, or the radial turning point of the mode.

Discussion

The unusual feature of this method, that the amount of computa-
tion is independent of the mode, is due to our extreme conservatism.
No advantage can be taken of the smoothness of low frequency modes or
of the shallow ray equivalent turning point of the high angular order,
low radial order mantle modes. On the other hand, as the computation
has been made practical, the luxury of such conservatism has done
away with troublesome special cases. Core modes and Stoneley modes
are as easy to compute as any other types.

Furthermore, this conservatism makes possible the solution of
the algebraic eigenvalue problem with the following advantages:

1) Highly accurate eigenfrequencies.

2) Correct computation of nearly coincident eigenfrequencies.

3) All modes in a frequency band are found.

4) No prior information about eigenfrequencies or eigenfunctions
is required.

The eigenvalue procedures routinely yield eigenvalues with
a precision on the order of a part in 10^{11} . However, the accuracy
of the eigenvalue is $O(h^6)$, $h = \max_i(x_{i+1} - x_i)$, and the accuracy
of the eigenfunction is $O(h^3)$ (Birkhoff, et al., 1969). For our
160 point grid " , we evaluated the accuracy emperically by comparing

eigenfrequencies between the variational program and a differential equation program (Alterman, Jarosch and Pekeris, 1959). The differential equation program was written with 10 decimal place constants and required a precision in the integration of one part in 10^8. The eigenvalues were identical to a relative accuracy of no less than one part in 10^7. Since these methods are philosophically very different, and algorithmically completely distinct, this result indicates to us that *both* programs are free of errors.

As a single example of the use of these methods we present, in Figure 1, the (ω, ℓ) diagram of spheroidal modes $(\omega \le 2\pi/45 \text{ sec}^{-1}$, $\ell \le 150)$ for model 1066B (Gilbert and Dziewonski, 1975).

Caption

Figure 1.   The spheroidal (ω, ℓ) diagram for Model 1066B

$(\omega \leq .14 \text{ sec.}^{-1}, \ell \leq 150)$. A continuous line joins

the points for each fixed value of the radial over-

tone number.

Fig. 1

1066B

D-10

ANGULAR ORDER

FREQUENCY (HOURS/DEG.)

Table 1

x	η_0	$\dot{\eta}_0$	ψ_0	$\dot{\psi}_0$
+1	0	0	0	0
0	1	0	0	1
-1	0	0	0	0

References

Alterman, Z., H. Jarosch, and C. L. Pekeris (1959). Oscillations of the Earth, *Proc. Roy. Soc. Lon.*, **A252**, 80-95.

Birkhoff, G., C. deBoor, B. Swartz, and B. Wendroff (1966). Raleigh-Ritz Approximation by Piecewise Cubic Polynomials, *SIAM J. Num. Anal.*, **3**, 188-203.

Courant, R. (1943). Variational Methods for the Solution of Problems of Equilibrium and Vibrations, *Bull. Amer. Math. Soc.*, **49**, 1-23.

Gilbert, F. and A. M. Dziewonski (1975). An Application of Normal Mode Theory to the Retrieval of Structural Parameters and Source Mechanisms from Seismic Spectra, *Phil Trans. Roy. Soc. Lon.*, **A278**, 187-269.

Martin, R. S., and J. H. Wilkinson (1967). Solution of Symmetric and Unsymmetric Band Equations and the Calculation of Eigenvectors of Band Matrices, *Num. Math.*, **9**, 279-301.

Pekeris, C. L. and H. Jarosch (1958). Free Oscillations of the Earth, *Contributions in Geophysics In Honor of Beno Gutenberg*, Pergamon Press, Los Angeles.

Peters, G. and J. H. Wilkinson (1969). Eigenvalues of $Ax = \lambda Bx$ with Band Symmetric A and B, *Comp. J.*, **12**, 398-404.

Wilkinson, J. H. (1965). *The Algebraic Eigenvalue Problem*, Clarendon Press, Oxford.

Research Note

The representation of seismic displacements in terms of traveling waves

Freeman Gilbert
Institute of Geophysics and Planetary Physics
Scripps Institution of Oceanography
University of California, San Diego
La Jolla, California   92037

Summary

The Poisson sum formula is used to transform the standing wave
representation of seismic displacements in a radially stratified sphere
into a traveling wave representation. The terms in the sum can be given
a physical interpretation, *via* the method of stationary phase, as classi-
cal wave packets making successive traversals of the great circle through
epicenter and receiver. The traveling wave representation forms the basis
for the retrieval of structural parameters and source mechanisms from the
spectra of traveling wave groups.

The representation of seismic displacements in terms of traveling waves

1. The traveling wave representation

The representation in terms of normal modes used by Gilbert and Dziewonski (1975, Sec. 2, hereafter referenced as M) is a standing wave representation. The sums over angular order can easily be converted into integrals over wavenumber from which a traveling wave representation can be obtained. Such a representation is desirable for the study of regional structure, for the separation of traveling wave orbits and overtones, and for the study of the moment rate tensor of regional events.

Suppose $U(r,\omega)$ is one component of the displacement spectrum for a particular radial overtone number, n , (M, [2.1.24,25])

$$U(r,\omega) = \sum_{\ell=0}^{\infty} a_\ell(r,\omega)\, C_\ell(\omega)$$

1)

$$a_\ell(r,\omega) = A_\ell(r) \cdot f(\omega)$$

and, for simplicity, suppose that $A_\ell(r)$ depends only on $P_\ell(\cos\theta)$

$$a_\ell(r,\omega) = h(\ell+\tfrac{1}{2}, r, \omega)\, P_\ell(\cos\theta)$$

2) $h(\ell+\tfrac{1}{2}, r, \omega) = H_\ell(r) \cdot f(\omega)$

$$A_\ell(r) = H_\ell(r)\, P_\ell(\cos\theta)$$

Then,

3) $\qquad U(r,\omega) = \sum_{\ell=0}^{\infty} h(\ell+\tfrac{1}{2}) \ P_{\ell}(\cos\theta) \ C_{\ell}(\omega)$

There are two steps to represent $U(r,\omega)$ in terms of traveling waves. The Poisson sum formula (Titchmarsh, 1948, p. 60; Nussenzweig, 1965, p. 27) is used to convert the sum in (3) into a series of integrals

4) $\qquad U(r,\omega) = \int_{0}^{\infty} d\lambda \sum_{k=-\infty}^{\infty} (-)^{k} \ h(\lambda) \ P_{\lambda-\frac{1}{2}}(\cos\theta) \ C(\lambda,\omega) \ e^{-i2k\pi\lambda}$

and zero is added to (4) in a suggestive manner. We use the Legendre function of the second kind, $Q_{\lambda-\frac{1}{2}}(\cos\theta)$, and rewrite the sum in (4)

5) $\qquad U(r,\omega) = \int_{0}^{\infty} d\lambda h(\lambda) \sum_{s=1}^{\infty} R_{s}(\lambda,\theta) \ C(\lambda,\omega)$

where

s- odd:

6)
$$R_{s}(\lambda,\theta) = (-)^{(s-1)/2} \left[P_{\lambda-\frac{1}{2}}(\cos\theta) \ \cos[(s-1)\pi\lambda] \right.$$
$$\left. + \frac{2}{\pi} Q_{\lambda-\frac{1}{2}}(\cos\theta) \ \sin[(s-1)\pi\lambda] \right]$$

s- even:

$$R_{s}(\lambda,\theta) = (-)^{s/2} \left[P_{\lambda-\frac{1}{2}}(\cos\theta) \ \cos(s\pi\lambda) \right.$$
$$\left. - \frac{2}{\pi} Q_{\lambda-\frac{1}{2}}(\cos\theta) \ \sin(s\pi\lambda) \right]$$

The term in (6) involving $Q_{\lambda-\frac{1}{2}}(\cos\theta)$ is zero for $s=1$, and the rest vanish in pairs $(2,3)$, $(4,5)$, etc., so that the terms in (5) involving $Q_{\lambda-\frac{1}{2}}(\cos\theta)$ sum to zero.

The reason for using (5) rather than (4) is that we can interpret $R_s(\lambda,\theta)$ in (5) and (6) as representing the sth passage, or orbit, of a traveling wave group. This interpretation is clarified by using the pair of functions (Nussenzweig, 1965, p. 89; Robin, 1958, pp. 237-240)

7) $\qquad Q_{\lambda-\frac{1}{2}}^{(1,2)}(\cos\theta) = \frac{1}{2}\left[P_{\lambda-\frac{1}{2}}(\cos\theta) \pm i\frac{2}{\pi}Q_{\lambda-\frac{1}{2}}(\cos\theta)\right]$

and rewriting (6) in the form

s- odd:

$$R_s(\lambda,\theta) = (-)^{(s-1)/2}\left[Q_{\lambda-\frac{1}{2}}^{(1)}(\cos\theta)e^{-i(s-1)\pi\lambda} + Q_{\lambda-\frac{1}{2}}^{(2)}(\cos\theta)e^{i(s-1)\pi\lambda}\right]$$

8)

s- even:

$$R_s(\lambda,\theta) = (-)^{s/2}\left[Q_{\lambda-\frac{1}{2}}^{(2)}(\cos\theta)e^{-is\pi\lambda} + Q_{\lambda-\frac{1}{2}}^{(1)}(\cos\theta)e^{is\pi\lambda}\right]$$

2. A physical interpretation

To understand the physical interpretation of $R_s(\lambda,\theta)$, as representing the sth passage of a traveling wave group, we use the method of stationary phase and the asymptotic approximations, valid for $\lambda\epsilon \gg 1$ and $\epsilon \leq \theta \leq \pi - \epsilon$,

9) $\qquad Q^{(1,2)}_{\lambda-\frac{1}{2}}(\cos\theta) = (2\pi\lambda\sin\theta)^{-\frac{1}{2}}\, e^{\mp i(\lambda\theta-\pi/4)}\,(1+0(\lambda^{-1}))$

Also we consider $f(\omega)$ to be a constant in (1) and (2). The actual behavior of f can be recovered by convolution in time or multiplication in frequency. In this case the temporal behavior $U(r,t)$ corresponding to (5) is $(M,(2.1.11))$

10) $\qquad U(r,t) = \int_0^\infty d\lambda h(\lambda) \sum_{s=1}^\infty R_s(\lambda,\theta)\left[\cos(\omega(\lambda)t)\, e^{-\alpha(\lambda)t} -1\right] H(t)$

In (10) we consider the transient term which we write as

11) $\qquad U(r,t) = \mathcal{R}e \int_0^\infty d\lambda h(\lambda) \sum_{s=1}^\infty R_s(\lambda,\theta)\, e^{i\omega(\lambda)t-\alpha(\lambda)t}$

Let us consider s- odd in (8)-(11) and let $U^{(1,2)}$ denote the contribution to U according as we use $Q^{(1,2)}_{\lambda-\frac{1}{2}}(\cos\theta)$ in (9). Then the integrand for $U^{(1,2)}$ has phase $\phi^{(1,2)}$

12) $\qquad \phi^{(1,2)} = \omega(\lambda)t \mp \lambda\left[(s-1)\pi + \theta\right] \pm \pi/4$

According to the method of stationary phase the dominant contributions to $U^{(1)}$ come from those values of λ for which $d\phi^{(1)}/d\lambda = 0$ or

13) $\qquad td\omega(\lambda)/d\lambda = (s-1)\pi + \theta = \Delta_s \geq 0$

If we define a group velocity $\gamma_s = \Delta_s/t$, in units, say, of radians/s., then (13) requires that

14) $\quad d\omega(\lambda)/d\lambda = \Delta_s/t = \gamma_s \geq 0$

in order that $\phi^{(1)}$ be stationary. For toroidal modes the variational formulation (Meissner, 1926) shows that $d\omega(\lambda)/d\lambda \geq 0$. Thus $\phi^{(1)}$ has at least one stationary value for some γ_s . For spheroidal modes it is almost always true that $d\omega(\lambda)/d\lambda \geq 0$. Some contrary examples have been given by Gilbert (1967).

The interpretation of Δ_s in (13) is that it is the total distance traveled by the wave group. The $s^{\underline{th}}$ wave group has traveled a distance θ from source to receiver plus an additional $(s-1)/2$ great circles in time t at group speed γ_s . This is exactly the interpretation given to the classical surface waves G_1 , R_3 , etc. Consequently, s corresponds exactly to the orbital index, 1, 3, $\cdot$ $\cdot$, for such a surface wave. In addition, the $s^{\underline{th}}$ term in (11), through the factor $(-)^{(s-1)/2}$ in (8), is out of phase with the $s \pm 2^{nd}$ term. This illustrates the polar phase shift (Brune, Nafe and Alsop, 1961). The $s^{\underline{th}}$ wave group has passed two more poles than the $s-2^{nd}$ wave group, and has its phase advanced $\pi/2$ twice.

Proceeding in a similar manner for $\phi^{(2)}$ in (12) we find the stationarity condition

15) $\quad d\omega(\lambda)/d\lambda = -\Delta_s/t = -\gamma_s \leq 0$

This condition is never met for toroidal modes and only rarely for spheroidal modes. Therefore, $U^{(2)}$ is of only minor importance, and is customarily neglected.

However, in (11) we could have used $\exp(-i\omega(\lambda)t)$ in place of $\exp(i\omega(\lambda)t)$. Then $U^{(2)}$ would have provided the dominant contribution and $U^{(1)}$ would have been negligable. That is, the dominant contribution to (11) for $\omega > 0$ and s- odd is $U^{(1,2)}$ according as the time behavior is taken to be $\exp(\pm i\omega t)$.

Considering s- odd in (8)-(11) shows that $R_s(\lambda,\theta)$ represents the $s\underline{th}$ traveling wave group. The group, of wavenumber λ and frequency $\omega(\lambda)$, travels a total distance Δ_s, given by (13), in time t at group speed γ_s. The important term in $R_s(\lambda,\theta)$ in (8) has superscript (1,2) according as the time behavior is $\exp(\pm i\omega t)$; $\omega > 0$.

Let us now consider s- even in (8)-(11), and let $U^{(1,2)}$ be the contribution to $U(r,t)$ according as we use $Q^{(1,2)}_{\lambda-\frac{1}{2}}(\cos\theta)$ in (9). The integrand for $U^{(1,2)}$ will have phase $\phi^{(1,2)}$

16) $\phi^{(1,2)} = \omega(\lambda)t \pm \lambda \left[s\pi-\theta\right] \pm \pi/4$

The phase $\phi^{(2)}$ has the stationarity condition

17) $td\omega(\lambda)/d\lambda = s\pi-\theta = \Delta_s > 0$

or

18) $d\omega(\lambda)/d\lambda = \Delta_s/t = \gamma_s \geq 0$

It is clear that the $s\underline{\text{th}}$ wave group travels the distance $2\pi - \theta$ from source to receiver plus an additional $(s-2)/2$ great circles in time t at group speed γ_s . The successive values of s correspond exactly to the orbital index 2, 4, $\cdot \cdot \cdot$, for such classical surface waves as G_2 , R_4 , etc. The polar phase shift between successive orbits is given by the factor $(-)^{s/2}$ in (8).

A consideration of $\phi^{(1)}$ leads to (15) with Δ_s given by (17), and $U^{(1)}$ is of only minor importance. The rôles of $U^{(1)}$ and $U^{(2)}$ are reversed if the integrand in (11) is replaced by its complex conjugate. That is, the important term in $R_s(\lambda, \theta)$ in (8) has superscript (2,1) according as the time behavior is $\exp(\pm i\omega t)$; $\omega > 0$.

The foregoing discussion, based on the method of stationary phase and the work of Brune, Nafe and Alsop (1961), illustrates that (5) is the exact traveling wave representation of seismic spectra. The functions $R_s(\lambda, \theta)$ in (8) represent traveling wave groups.

3. The standard form

At this point it is desirable to put (5) into a form similar to (2.1.24) and (2.1.25) of M . Using Legendre functions of the second kind

19) $\qquad Q_{\lambda - \frac{1}{2}}^{m(1,2)}(\cos \theta) = \frac{1}{2} \left[P_{\lambda - \frac{1}{2}}^m(\cos \theta) \pm i \frac{2}{\pi} Q_{\lambda - \frac{1}{2}}^m(\cos \theta) \right]$

we introduce the functions $R_s^m(\lambda, \theta)$

s- odd:

$$R_s^m(\lambda,\theta) = (-)^{(s-1)/2} \left[Q_{\lambda-\frac{1}{2}}^{m(1)}(\cos\theta) e^{-i(s-1)\pi\lambda} + Q_{\lambda-\frac{1}{2}}^{m(2)}(\cos\theta) e^{i(s-1)\pi\lambda} \right]$$

20)

s- even:

$$R_s^m(\lambda,\theta) = (-)^{s/2} \left[Q_{\lambda-\frac{1}{2}}^{m(2)}(\cos\theta) e^{-is\pi\lambda} + Q_{\lambda-\frac{1}{2}}^{m(1)}(\cos\theta) e^{is\pi\lambda} \right]$$

and we define

21)
$$X_s^m(\lambda,\theta) = (-)^m (\lambda/2\pi)^{\frac{1}{2}} \begin{Bmatrix} 1 \\ (\lambda^2-\frac{1}{4})^{-\frac{1}{2}} \\ (\lambda^2-\frac{1}{4})^{-\frac{1}{2}}(\lambda^2-9/4)^{-\frac{1}{2}} \end{Bmatrix} R_s^m(\lambda,\theta)$$

according as $m = 0$, 1 , 2 . The second and third terms in braces in (21) can be well approximated by λ^{-1} and λ^{-2} , respectively, for $\lambda \gg 1$. We now define $A_s(\lambda,r)$ in terms of (21) exactly as A is defined in (2.1.30) and (2.1.31) of M in terms of $X_\ell^m(\theta)$. Note: the sign of A_{36} in M(2.1.31) should be negative.

Thus, we can write the traveling wave representation, generalizing (5), as

22)
$$U(r,\omega) = \int_0^\infty d\lambda \sum_{s=1}^\infty a_s(\lambda,r)\, C(\lambda,\omega); \quad a_s(\lambda,r) = A_s(\lambda,r) \cdot f(\omega)$$

The traveling wave representation (22) forms the basis for the retrieval of structural parameters and source mechanisms from the frequency spectra of traveling wave groups. It also forms the basis

for an investigation of body waves (Burridge, 1966; Ansell, 1973),
where $A_s(\lambda,r)$ is decomposed into a series of terms, each of which
represents a generalized ray (Brune, 1964; Ben-Menahem, 1964).

4. Transition to plane stratification

The representation in terms of traveling waves for a plane
stratified medium can be obtained from the foregoing expressions by a
limiting process. Let $x = a\theta$ where a is the radius of the sphere
for which we have the traveling wave representation. Let x, the
epicentral distance, be fixed. Let $\lambda = ka$, where k is the (fixed)
wave number on the surface. Then the representation for a plane strati-
fied medium is found as the limit as $a \to \infty$ of the representation for a
sphere. We use the uniform asymptotic approximations of Szegö (1934)
that permit us to replace (9) by (23) for large λ

$$23) \qquad Q_{\lambda-\frac{1}{2}}^{(1,2)}(\cos\theta) = \tfrac{1}{2}(\theta/\sin\theta)^{\frac{1}{2}} H_0^{(2,1)}(\lambda\theta)\left(1+O(\lambda^{-1})\right); \quad \theta \le \pi/2$$

in terms of Hankel functions.

The terms for $s > 1$ in (5) represent wave groups that arrive
at successively later times, $\quad t_s$, where t_s is the earliest group
arrival time for the $s\underline{\text{th}}$ group. Since $\lim\limits_{a\to\infty} t_s = \infty$, because each
group must travel a distance of at least πa, we shall consider only
$s = 1$ in (5)

$$24) \qquad U(r,\omega) = \int_0^\infty d\lambda\, h(\lambda)\, R_1(\lambda,\theta)\, C(\lambda,\omega)$$

Combining (23) and (8) gives

$$R_1(\lambda,\theta) = \tfrac{1}{2}(\theta/\sin\theta)^{\frac{1}{2}} \left[H_0^{(2)}(\lambda\theta) + H_0^{(1)}(\lambda\theta) \right]$$

25)

$$= (\theta/\sin\theta)^{\frac{1}{2}} J_0(\lambda\theta)$$

The product $\lambda\theta$ in (25) is the same as kx

26) $\quad R_1(\lambda,\theta) = (\theta/\sin\theta)^{\frac{1}{2}} J_0(kx)$

As $\theta \to 0$ ($a \to \infty$) (24) becomes

27) $\quad U(r,\omega) = a \int_0^\infty dk\ h(ka)\ J_0(kx)\ C(k,\omega)$

A careful analysis of h , including the normalizing integral (M, (2.1.3)) shows that h is $O(a^{-1})$ so that $\lim\limits_{a\to\infty}$ of (27) is finite.

The presence of the cylindrical Bessel function in (27) in place of the spherical harmonic, the Legendre function, in (1) and (2), illustrates the transition from spherical stratification to plane stratification.

Acknowledgements

References

Ansell, J. H., 1973, Legendre functions, the Hilbert transform and surface waves on a sphere. *Geophys. J. R. astr. Soc.*, **32**,

Ben-Menahem, A., 1964, Mode-ray duality. *Bull. Seism. Soc. Am.*, **54**, 1315-1321.

Brune, J. N., 1964, Travel times, body waves, and normal modes of the Earth. *Bull. Seism. Soc. Am.*, 54, 2099-2128.

Brune, J. N., Nafe, J. E. and Alsop, L. E., 1961, The polar phase shift of surface waves on a sphere. *Bull. Seism. Soc. Am.*, 51, 247-257.

Burridge, R., 1966, The Legendre function of the second kind with complex argument in the theory of wave propagation. *J. Math. Phys.*, **45**, 322-330.

Gilbert, F., 1967, Gravitationally perturbed elastic waves. *Bull. Seism. Soc. Am.*, 57, 783-794.

Gilbert, F., and Dziewonski, A. M., 1975, An application of normal mode theory to the retrieval of structural parameters and source mechanisms from seismic spectra. *Phil. Trans. Roy. Soc. Lon.*, A278, 187-269.

Meissner, E., 1926, Elastische Oberflächen-Querwellen. *Proc. 2nd Intern. Congr. Appl. Mech., Zurich*, 3-11.

Nussenzweig, H. M., 1965, High-frequency scattering by an impenetrable sphere. *Ann. Phys. (N.Y.)*, 34, 23-95.

Robin, L., 1958, *Fonctions Sphériques de Legendre et Fonctions Sphéroïdales*, t. 2, Gauthier-Villars, Paris.

Szegö, G., 1934, Über einige asymptotische Entwicklungen der Legendreschen Funktionen. *Proc. Lon. Math. Soc.*, (2)36, 427-450.

Titchmarsh, E. C., 1948, *Introduction to the Theory of Fourier Integrals*, 2nd ed., Clarendon Press, Oxford.